Biophysical Properties and Slow Voltage-dependent Inactivation of a Sustained Sodium Current in Entorhinal Cortex Layer-II Principal Neurons
A Whole-Cell and Single-Channel Study

Jacopo Magistretti*‡ and Angel Alonso*

From the *Department of Neurology and Neurosurgery, McGill University and Montreal Neurological Institute, Montréal, Québec, H3A 2B4 Canada; and ‡Dipartimento di Neurofisiologia Sperimentale, Istituto Nazionale Neurologico "Carlo Besta", 20133 Milano, Italy

abstract The functional and biophysical properties of a sustained, or "persistent," Na^+ current (I_{NaP}) responsible for the generation of subthreshold oscillatory activity in entorhinal cortex layer-II principal neurons (the "stellate cells") were investigated with whole-cell, patch-clamp experiments. Both acutely dissociated cells and slices derived from adult rat entorhinal cortex were used. I_{NaP}, activated by either slow voltage ramps or long-lasting depolarizing pulses, was prominent in both isolated and, especially, in situ neurons. The analysis of the gating properties of the transient Na^+ current (I_{NaT}) in the same neurons revealed that the resulting time-independent "window" current (I_{NaTW}) had both amplitude and voltage dependence not compatible with those of the observed I_{NaP}, thus implying the existence of an alternative mechanism of persistent Na^+-current generation. The tetrodotoxin-sensitive Na^+ currents evoked by slow voltage ramps decreased in amplitude with decreasing ramp slopes, thus suggesting that a time-dependent inactivation was taking place during ramp depolarizations. When ramps were preceded by increasingly positive, long-lasting voltage prepulses, I_{NaP} was progressively, and eventually completely, inactivated. The $V_{1/2}$ of I_{NaP} steady state inactivation was approximately −49 mV. The time dependence of the development of the inactivation was also studied by varying the duration of the inactivating prepulse: time constants ranging from ∼6.8 to ∼2.6 s, depending on the voltage level, were revealed. Moreover, the activation and inactivation properties of I_{NaP} were such as to generate, within a relatively broad membrane-voltage range, a really persistent window current (I_{NaPW}). Significantly, I_{NaPW} was maximal at about the same voltage level at which subthreshold oscillations are expressed by the stellate cells. Indeed, at −50 mV, the I_{NaPW} was shown to contribute to >80% of the persistent Na^+ current that sustains the subthreshold oscillations, whereas only the remaining part can be attributed to a classical Hodgkin-Huxley I_{NaTW}. Finally, the single-channel bases of I_{NaP} slow inactivation and I_{NaPW} generation were investigated in cell-attached experiments. Both phenomena were found to be underlain by repetitive, relatively prolonged late channel openings that appeared to undergo inactivation in a nearly irreversible manner at high depolarization levels (−10 mV), but not at more negative potentials (−40 mV).

key words: persistent Na^+ current • window current • stellate cells • oscillations • patch clamp

INTRODUCTION

The so-called persistent sodium current (I_{NaP})[1] is known to be expressed, together with the classical, transient sodium current (I_{NaT}), by numerous mammalian neuronal types. Its basic features include persistence during prolonged depolarizations, lower threshold of activation than I_{NaT}, and low amplitude (the underlying conductance normally representing 0.2–2% of the total sodium conductance; French and Gage, 1985; French et al., 1990; for review see Taylor, 1993; Crill, 1996. After the initial descriptions of the actions of sustained Na^+ currents on neuronal electroresponsiveness (Hotson et al., 1979; Llinás and Sugimori, 1980; Connors et al., 1982), I_{NaP} was first demonstrated with voltage-clamp studies in neocortical neurons (Stafstrom et al., 1982, 1985), and biophysically characterized in the hippocampus (French and Gage, 1985; French et al., 1990). I_{NaP} has also been observed, directly or indirectly, in an increasing number of neuronal structures including basal ganglia (Chao and Alzheimer, 1995; Cepeda et al., 1995), amygdala (Pape and Driesang, 1998), thalamus (Jahnsen and Llinás, 1984; Parri and Crunelli, 1998), hypothalamus (Llinás and Alonso, 1992; Uteshev et al., 1995), cerebellum (Jahnsen, 1986; D'Angelo et al., 1998; Kay et al., 1998), and peripheral ganglia (Baker and Bostock, 1997). Due

Portions of this work were previously published in abstract form (Magistretti, J., and A. Alonso. 1998. NYAS Meetings. Abstr. No. PI–29; Alonso, A., and J. Magistretti. 1998. *Soc. Neurosci. Abstr.* 24:2035).

Address correspondence to Prof. Angel Alonso, Department of Neurology and Neurosurgery, Montreal Neurological Institute, McGill University, 3801 University Street, Montréal, Québec, H3A 2B4 Canada. Fax: (514) 398-8106; E-mail: mdao@musica.mcgill.ca

[1]*Abbreviations used in this paper:* 4-AP, 4-aminopyridine; EC, entorhinal cortex; I_{NaP} and G_{NaP}, persistent Na^+ current and conductance; I_{NaPW} and G_{NaPW}, window current and conductance resulting from G_{NaP}; I_{NaT} and G_{NaT}, transient Na^+ current and conductance; I_{NaTW} and G_{NaTW}, window current and conductance resulting from G_{NaT}; I–V, current–voltage; TEA, tetraethylammonium; TTx, tetrodotoxin.

J. Gen. Physiol. © The Rockefeller University Press • 0022-1295/99/10/491/19 $5.00
Volume 114 October 1999 491–509
Available online 13 September 1999
http://www.jgp.org

to its voltage-dependent properties, I_{NaP} can contribute to important integrative functions such as amplification of excitatory postsynaptic potentials (Deisz et al., 1991; Stuart and Sakmann, 1995; Schwindt and Crill, 1995; Lipowsky et al., 1996), generation of pacemaker activity (Alonso and Llinás, 1989; Amitai, 1994; Pennartz et al., 1997; Pape and Driesang, 1998), and firing-pattern shaping (Jahnsen and Llinás, 1984; Klink and Alonso, 1993; Franceschetti et al., 1995; Parri and Crunelli, 1998). Since I_{NaP} can generate membrane bistability and plateau potentials, it has also been implicated in the pathogenesis of some forms of epilepsy (Segal, 1994; for review see Ragsdale and Avoli, 1998). In addition, the ability of I_{NaP} to sustain long-lasting Na^+ influxes, and therefore to steadily increase intracellular Na^+ concentration, has raised interest as to its possible role in mechanisms of neurodegeneration (Taylor and Meldrum, 1995).

The entorhinal cortex (EC) has proven to be a particularly interesting neuronal system for the study of I_{NaP} functions. In the stellate cells of EC layer II, which give rise to the main cortical projection to the hippocampus (Steward and Scoville, 1976), I_{NaP} has been shown to critically participate in the generation of subthreshold membrane-potential oscillations in the theta-rhythm range (Alonso and Llinás, 1989; Klink and Alonso, 1993). This particular intrinsic subthreshold activity is considered to be a critical determinant for the generation of the population theta oscillations generated by the EC network (Adey et al., 1957, 1960; Holmes and Adey, 1960; Mitchell and Ranck, 1980; Alonso and García-Austt, 1987a,b). The theta rhythm has been shown to contribute to synaptic-plasticity processes (Larson and Lynch, 1986; Larson et al., 1986; Greenstein et al., 1988; Alonso et al., 1990; Huerta and Lisman, 1996; Hölscher et al., 1997), and it is thus believed to play a major role in temporal lobe learning and memory functions (Doyère and Laroche, 1992; Buzsáki, 1996). On the other hand, since the EC is also known to play a crucial role in temporal lobe epileptogenesis (see references in Dickson and Alonso, 1997), it has been hypothesized that the presence of a robust I_{NaP} in EC neurons may contribute to epileptogenic processes (Klink and Alonso, 1993).

For the above considerations, a detailed knowledge of the biophysical properties of I_{NaP} expressed by EC layer II neurons seems of great interest since it would help to understand how this current specifically influences the physiological behavior of these cells. In this study, we have characterized I_{NaP} in both acutely isolated and in situ EC layer II neurons. Our results revealed the existence of some interesting biophysical properties of I_{NaP} that had not been thoroughly investigated yet, including: (a) a slow voltage- and time-dependent inactivation occurring with voltage-dependent time constants in the order of seconds; (b) a full inactivation at sufficiently positive potentials; and (c) a truly persistent, or "window," current arising from the particular activation and steady state inactivation properties of the corresponding conductance. Moreover, we describe the single-channel events that account for all of the above-mentioned macroscopic phenomena.

MATERIALS AND METHODS

Slice and Cell Preparation

Young-adult Long-Evans rats (P25–P35) were killed by decapitation. The brain was quickly removed under hypothermic conditions, blocked on the stage of a vibratome (Pelco), and submerged in an ice-cold cutting solution containing (mmol/liter): 115 NaCl, 5 KCl, 4 $MgCl_2$, 1 $CaCl_2$, 20 PIPES, and 25 d-glucose, pH 7.4 with NaOH, bubbled with pure O_2. Osmotic pressure (π) of the latter solution, as measured with a Micro Osmette 5004 osmometer, was typically 320 mOsm. Horizontal slices of the retrohippocampal region were cut at 350–400 μm. For in situ recordings, slices were stored at room temperature in the above solution until use. For recordings on isolated neurons, the layer II of medial entorhinal cortex was dissected from each slice (White et al., 1993). Neurons were acutely isolated from the tissue fragments thus obtained following an enzymatic and mechanical dissociation procedure described elsewhere (Magistretti and de Curtis, 1998).

Whole-Cell Recordings on Slices

The recording chamber was mounted on the stage of an upright microscope (see below). Slices were laid onto the bottom of the chamber and perfused with an extracellular solution containing (mmol/liter): 34 NaCl, 26 $NaHCO_3$, 80 tetraethylammonium (TEA)-Cl, 5 KCl, 3 CsCl, 2 $CaCl_2$, 3 $MgCl_2$, 2 $BaCl_2$, 2 $CoCl_2$, 0.4 $CdCl_2$, 4 4-aminopyridine (4-AP), 10 glucose, pH 7.4 when bubbled with 95% O_2, 5% CO_2 ($\pi \approx 320$ mOsm). The association of Co^{2+} and Cd^{2+} was found to depress residual inward rectification insensitive to the application of tetrodotoxin (TTx; Sigma-Aldrich Canada Ltd.) more effectively than Cd^{2+} alone in slices (but not in freshly dissociated neurons; see below). Preliminary experiments were performed in in situ neurons in the absence of extracellular Co^{2+} and Ba^{2+} and in the presence of 0.2 rather than 0.4 mM Cd^{2+}. Both average peak amplitude and current density of ramp (50 mV/s)-evoked, TTx-subtracted I_{NaP}s recorded under the former and latter ionic conditions (-179.3 ± 120.7 vs. -195.8 ± 100.0 pA, respectively, and -17.7 ± 29.1 vs. -12.9 ± 10.6 pA/pF, respectively, $n = 54$ and 8, respectively) were not significantly different ($P = 0.68$ and 0.63, respectively). Hence, possible enhancing effects of nonphysiological extracellular divalent cations on I_{NaP} amplitude (Cummins et al., 1998) did not significantly affect measures in our experimental conditions. Patch pipettes were fabricated from thick-wall borosilicate glass capillaries by means of a P-97 horizontal puller (Sutter Instruments Co.). The intrapipette solution contained (mmol/liter): 110 CsF, 10 HEPES-Na, 11 EGTA, 2 $MgCl_2$, pH 7.25 with CsOH (π adjusted to $\sim$290 mOsm with mannitol). When filled with the above solution, the patch pipettes had a resistance of 3–5 MΩ. Slices were observed with an Axioskop microscope (Carl Zeiss, Inc.) equipped with a 40$\times$ water-immersion objective lens and differential-contrast optics. A near-infrared charge-coupled device camera (XC-75; Sony Corp.) was also connected to the microscope, and used to improve cell visualization for identification of neuron types and during the approaching and patching procedures. With this equipment, the principal cells of EC layer II were easily distinguished based on their somato-dendritic shape

(stellate cells: Ramón y Cajal, 1902), size, and position (Klink and Alonso, 1997). Patch pipettes were brought in close proximity to the selected neurons while manually applying positive pressure inside the pipette. Tight seals (>100 GΩ) and the whole-cell configuration were obtained by suction (Hamill et al., 1981). Series resistance (R_s) was always compensated by ~55% with the amplifier's built-in compensation section. R_s, as estimated off-line from the peak amplitude of averaged capacitive transients evoked by −5-mV voltage square pulses (with the low-pass filter set at 10 kHz), was on average 8.5 ± 2.1 MΩ (n = 54). Cell capacitance was evaluated online by canceling the fast component of whole-cell capacitive transients evoked by −10-mV voltage steps with the amplifier compensation section, and reading out the corresponding value. Voltage-clamp recordings were performed at room temperature (~22°C) using an Axopatch 1D amplifier (Axon Instruments). The general holding potential was −80 mV.

Whole-Cell Recordings on Isolated Neurons

The recording chamber was mounted on the stage of an inverted microscope (see below). After seeding into the chamber, dissociated cells were perfused with a standard HEPES buffer containing (mmol/liter): 140 NaCl, 5 KCl, 10 HEPES (free acid), 2 $CaCl_2$, 2 $MgCl_2$, 25 glucose, pH 7.4 with NaOH, bubbled with pure O_2 ($\pi \approx 320$ mOsm). After wash-out of cell debris, cell perfusion was switched to a solution suitable for Na^+-current isolation containing (mmol/liter): 100 NaCl, 40 TEA-Cl, 10 HEPES (free acid), 2 $CaCl_2$, 3 $MgCl_2$, 0.2 $CdCl_2$, 5 4-AP, 25 glucose, pH 7.4 with NaOH, bubbled with pure O_2 ($\pi \approx 318$ mOsm). The intrapipette solution was the same as described in the previous paragraph. Cells were observed at 400× with an Axiovert 100 microscope (Carl Zeiss, Inc.). After tight-seal formation (>100 GΩ) and the establishment of the whole-cell configuration, series resistance was on average 12.0 ± 4.5 MΩ (n = 38), and was always compensated by ~70%. The remaining procedures and experimental conditions were the same as described in the previous paragraph.

Single-Channel Recordings

Single-channel, cell-attached experiments were performed in acutely isolated neurons. After seeding into the recording chamber, cells where initially perfused with the same solution as described in the previous paragraph. The pipette solution contained (mmol/liter): 130 NaCl, 35 TEA-Cl, 10 HEPES-Na, 2 $CaCl_2$, 2 $MgCl_2$, 5 4-AP, pH 7.4 with HCl ($\pi \approx 338$ mOsm). Single-channel patch pipettes had resistances ranging from 10 to 35 MΩ when filled with the above solution, and were always coated with Sylgard® (Dow Corning Corp.) from the shoulder to a point as close as possible to the tip so as to minimize stray pipette capacitance. After obtaining the cell-attached configuration, the extracellular perfusion was switched to a high-potassium solution containing: 140 K-acetate, 5 NaCl, 10 HEPES (free acid), 4 $MgCl_2$, 0.2 $CdCl_2$, 25 glucose, pH 7.4 with KOH ($\pi \approx 320$ mOsm) so as to hold the neuron resting membrane potential at or near 0 mV. Recordings were performed at room temperature with an Axopatch 200B amplifier (Axon Instruments). Capacitive transients and linear current leakage were minimized online by acting on the respective built-in compensation sections of the amplifier. Long-duration (20-s) depolarizing voltage steps were delivered one every 40 s from a holding potential of −80 or −100 mV.

Data Acquisition

Voltage protocols were commanded and current signals were acquired with a Pentium PC interfaced to an Axon TL1 interface, using the Clampex program of the pClamp 6.0.2 software (Axon Instruments). Current signals were filtered online (using the amplifier's built-in low pass filter) and digitized at different frequencies according to the specific experimental aim. Filtering and acquisition frequencies were 5 and 20 kHz, respectively, for I_{NaT} recordings; 0.1–1 and 0.67–10 kHz (depending on the protocol duration), respectively, for I_{NaP} recordings; 1 and 2 kHz, respectively, for single-channel recordings. In all of the voltage protocols applied, cell-membrane potential was kept at the holding level for 15 (in whole-cell experiments) or 20 s (in single-channel experiments) between the end of each sweep and the beginning of the subsequent sweep (or of the conditioning prepulse preceding it, when applied). This avoided the development of cumulative voltage-dependent inactivation of I_{NaP} during consecutive acquisition cycles.

Data Analysis

Whole-cell recordings were analyzed by means of the Clampfit program (Axon Instruments). Offline leak subtraction was performed on I_{NaT}- (but not I_{NaP}-) protocol traces. Current density was calculated by dividing the peak current amplitude by cell capacitance, estimated as explained above. Conductance values were calculated from Na^+-current amplitudes by applying the extended Ohm's law in the form: $G_{Na} = I_{Na}/(V - V_{Na})$, where V_{Na} is the nominal (Nernst) Na^+ reversal potential. Data were fitted with exponential functions, $I = (A_i \cdot \exp(-t/\tau_i) + C$, using Clampfit, or with Boltzmann functions, $G = G_{max}/\{1 + \exp[(V - V_{1/2})/k)]\}$, using Origin 3.06 (MicroCal Software).

Single-channel recordings were analyzed using Clampfit, Fetchan, and pStat (Axon Instruments). Residual capacitive transients were nullified by offline subtracting fits of average blank traces. Residual leakage currents were carefully measured in every single sweep at trace stretches devoid of any channel openings, and digitally subtracted. Channel dwell times were determined using a standard threshold routine of the Fetchan program. Ensemble-average traces were fitted with single exponential functions, $I = A \cdot \exp(-t/\tau) + C$, using Clampfit. Dwell-time histograms were fitted with double exponential functions, $N = A_1 \cdot \exp(-t/\tau_1) + A_2 \cdot \exp(-t/\tau_2)$, using pStat.

Average values were expressed as mean ± SD, unless otherwise explicitly stated. Statistical significance was evaluated by means of the two-tail Student's t test for unpaired data.

Modeling I_{NaP}

For a phenomenological description of I_{NaP} activation and slow inactivation, a simple Hodgkin-Huxley model was assumed. We applied the basic relationship:

$$I_{NaP}(V, t) = G_{NaP}(V, t) \cdot (V - V_{Na}), \quad (1)$$

where

$$G_{NaP}(V, t) = G_{NaP(max)} \cdot m_\infty(V) \cdot h(V, t), \quad (2)$$

and m and h are the probabilities of the activating and inactivation particles, respectively, to be in the permissive position. I_{NaP} activation was assumed to be instantaneous, and $m_\infty(V)$ was derived directly from the G_{NaP} activation curve. $h_\infty(V)$ was derived directly from the G_{NaP} steady state inactivation curve. The transitions of the inactivating particle, h, were modeled according to the following first-order kinetic scheme:

$$1 - h \underset{\beta}{\overset{\alpha}{\Leftrightarrow}} h$$

from which it follows:

$$h(V, t) = h_\infty(V) - [h_\infty(V) - h_0] \cdot \exp(-t/\tau_h), \quad (3)$$

where

$$\tau_h(V) = 1/[\alpha(V) + \beta(V)] \quad (4)$$

and

$$h_\infty(V) = \alpha(V)/[\alpha(V) + \beta(V)]. \quad (5)$$

Numerical values for the rate constants, α and β, were derived from the experimental values of time constants of inactivation and recovery from inactivation (τ_h) and from the h_∞ curve by applying Eqs. 4 and 5. After obtaining the analytical functions describing the voltage dependence of the rate constants (see results), the time course of I_{NaP}s activated in response to various voltage protocols was numerically reconstructed on the basis of the Eqs. 1 and 2, and Eq. 3 in its differential form. The simulation programs were compiled using QuickBASIC 4.5 (Microsoft Corp.).

RESULTS

General Properties of I_{NaP} in Acutely Dissociated and In Situ Neurons

In acutely dissociated EC layer II principal neurons, a prominent I_{NaP} could be evoked by delivering long-lasting depolarizing pulses. Fig. 1 A illustrates current traces from a representative neuron. I_{NaP} was blocked by 1 μM TTx, and was therefore routinely isolated via TTx subtraction. I_{NaP} threshold of activation was at about −65 mV, and peak at −30 mV. Average I_{NaP} absolute amplitude (derived by averaging the data points between 400 and 500 ms from the pulse onset) and current density (calculated as explained in materials and methods) were −96.5 ± 61.5 pA and −12.0 ± 7.0 pA/pF, respectively, at the peak of the current-voltage (I–V) relationship (n = 5). The average I_{NaP} I–V relationship showed a linear region from −30 to −5 mV, the linear best fitting of which returned a zero-current level at +63.0 mV (not shown). This value compares favorably with the theoretical Nernst Na^+ reversal potential calculated for our ionic conditions (V_{Na} = +61.0 mV). The voltage dependence of the conductance underlying I_{NaP} (G_{NaP}, calculated as explained in the materials and methods) is shown in the average plot of Fig. 1 A, inset. Boltzmann fitting to data points returned a half-activation voltage, $V_{1/2}$, of −44.4 mV, and a slope factor, k, of −5.2 mV. The ratio between the peak G_{NaP} value

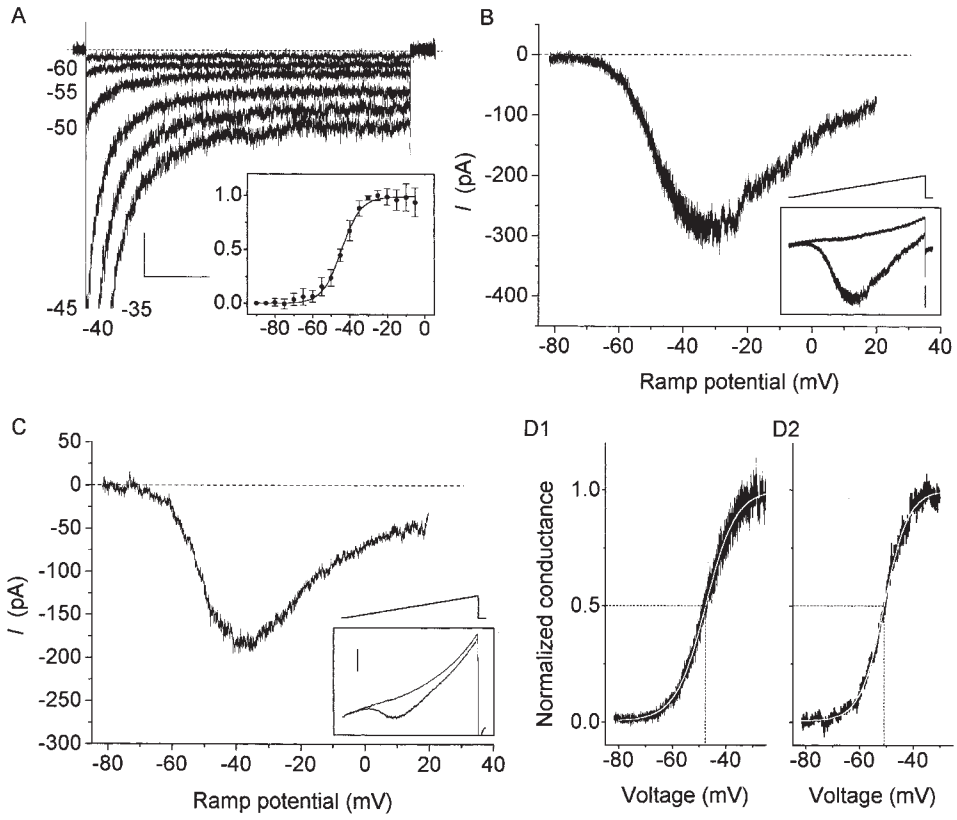

Figure 1. Basic features of I_{NaP} in EC layer II principal neurons. (A) I_{NaP}s evoked in a representative acutely isolated neuron (cell E6M15) by 500-ms depolarizing square pulses at −65 to −35 mV. All the traces shown are TTx subtracted (control minus 1 μM TTx). The holding potential was −80 mV. Scale bars: 100 pA, 100 ms. (Inset) Average plot of normalized G_{NaP} derived, as explained in materials and methods, from step protocols (I_{NaP} amplitude was measured by averaging the data points between 400 and 500 ms from the pulse onset; n = 5). The best Boltzmann fitting to data points is also shown. Fitting parameters were: $V_{1/2}$ = −44.4 mV, k = −5.2 mV. (B and C) I_{NaP}s evoked in a representative acutely isolated neuron (B; cell A6M15) and a representative in situ neuron (C; cell D7904) by slow voltage ramps (50 mV/s, from −80 to +20 mV; the voltage protocol is schematized above the insets). The currents shown in the main panels have been obtained by digitally subtracting the traces recorded in 1 μM TTx from control traces (both shown in the insets; calibration bars: 100 pA in B, 200 pA in C). (D) Plots of the voltage dependence of activation of I_{NaP} in the same two neurons as shown in B and C (D1 and D2, respectively). Na^+ conductances (G_{NaP}s) were derived from the early parts of the TTx-subtracted currents by applying the extended Ohm equation (materials and methods). G_{NaP} plots were normalized for the maximal values and fitted with single Boltzmann functions (empty lines). Fitting parameters were: $V_{1/2}$ = −47.6 mV, k = −5.5 mV (D1); $V_{1/2}$ = −50.8 mV, k = −4.5 mV (D2). The perpendicular, dotted lines indicate the half-maximal activation and the corresponding $V_{1/2}$.

found in each cell and the maximal value of the conductance underlying the transient Na^+ current (I_{NaT}) expressed by the same cell was also calculated, and averaged 0.0187 ± 0.0097 ($n = 5$).

To quickly explore the whole voltage range of I_{NaP} activation, ramp protocols were then used. Slow ramps at 50 mV/s were initially selected since they allowed full inactivation of fast-decaying Na^+-current component(s). Fig. 1 B shows the currents evoked by such a protocol in a representative acutely dissociated neuron, both in control conditions and in the presence of 1-μM TTx (inset). Offline digital subtraction returned the TTx-sensitive I_{NaP} in isolation (Fig. 1 B). The continuous I–V relationship thus obtained showed a threshold at −70/−60 mV and a peak at −40/−30 mV. Noteworthy in both pulse and ramp protocols, I_{NaP} activation was accompanied by an evident increase in current noise, especially at voltage levels close to the peak of the I–V relationship (Fig. 1, A and B), consistent with the relatively high conductance (∼20 pS) characterizing the channels responsible for I_{NaP} generation in EC layer II neurons (Magistretti et al., 1999).

Ramp protocols were also used in experiments performed in in situ neurons. In this situation, TTx subtraction always returned prominent I_{NaP}s in isolation, whose I–V relationship closely resembled that of I_{NaP}s in acutely dissociated neurons (Fig. 1 C). I_{NaP} amplitude, measured at the peak of the I–V relationship, was significantly higher in in situ than in isolated neurons (−179.3 ± 120.7 pA, $n = 54$, vs. −65.6 ± 37.9 pA, $n = 38$; $P < 5 \times 10^{-7}$), whereas the current density did not significantly differ in the two situations (−17.7 ± 29.1 pA/pF, $n = 54$, vs. −16.5 ± 8.6 pA/pF, $n = 38$; $P = 0.8$). These findings strongly suggest that the channels responsible for I_{NaP} are located not only on the soma, but also on neuronal processes severed by the dissociation procedure. Activation curves of I_{NaP}s recorded in both in situ and isolated neurons were also constructed. Conductance values were derived from I_{NaP}s by applying the extended Ohm's law (see materials and methods), and the resulting activation curves were fitted with single Boltzmann functions (Fig. 1 D). Average half-activation potentials and slope factors were very similar in in situ neurons ($V_{1/2} = -51.3 \pm 3.9$ mV, $k = -4.0 \pm 0.7$ mV, $n = 39$) and isolated neurons ($V_{1/2} = -48.7 \pm 4.7$ mV, $k = -4.4 \pm 0.9$ mV, $n = 19$). These values compare favorably with those obtained from step protocols (see above), and are also in good agreement with the activation parameters previously reported for I_{NaP}s expressed in other neuronal systems (French et al., 1990; Brown et al., 1994; Baker and Bostock, 1997).

Given the effectiveness of TTx subtraction in isolating I_{NaP}s in both isolated and in situ neurons, this procedure was routinely used in our study. All of the data presented from this point on are from TTx-subtracted currents.

I_{NaP} Is Not a Window Current Generated by Transient Na^+ Channels

It is well known that a noninactivating, "window" current (I_{NaTW}) can be generated by the gating properties of fast, transient Na^+ channels (Hodgkin and Huxley, 1952). To address the issue of whether the I_{NaP} expressed by EC layer II neurons can be accounted for by a classical window conductance, we analyzed the voltage-dependence properties of I_{NaT} in acutely dissociated neurons. Fig. 2 A shows Na^+-current traces recorded in a representative neuron in response to an activation–inactivation pulse protocol. Peak-current amplitudes were measured and used for deriving conductance values (G_{NaT}); normalized activation and steady state inactivation plots were then constructed (Fig. 2 B), and fitted with Boltzmann functions. The optimal approximation to data points returned by single Boltzmann functions suggested the existence of functionally homogeneous, transient Na^+ channels in the neuronal preparation under examination. In eight cells, average $V_{1/2}$ and k were −32.5 ± 6.5 mV and −3.6 ± 0.9 mV, respectively, for the activation function, and −59.8 ± 5.2 mV and 4.5 ± 0.9 mV, respectively, for the steady state inactivation function. These values are similar to those reported in a number of other studies on neuronal I_{NaT} voltage dependence (e.g., Sah et al., 1988; Huguenard et al., 1988; Cummins et al., 1994). The product of the activation and steady state inactivation functions was then calculated in individual cells to derive the theoretically predicted voltage dependence of the window conductance (G_{NaTW}) arising from transient Na^+ channels (Fig. 2 B, dotted line). Fig. 2 C illustrates the I_{NaP} evoked by a standard ramp protocol, and isolated via TTx subtraction, in the same cell as in A and B. The conductance underlying I_{NaP} (G_{NaP}) was calculated and compared with the predicted G_{NaTW} (Fig. 2 D); an evident discrepancy in the voltage dependence of the two conductances could be observed at potentials positive to about −30 mV, where G_{NaTW} rapidly fell towards zero, whereas G_{NaP} maintained relatively high values, though it also showed a characteristic decline from its maximum (see below). The same discrepancy between G_{NaTW} and G_{NaP} was observed in four other acutely dissociated neurons, in which both well-clamped I_{NaT}s and sizable I_{NaP}s could be recorded. In a broader cell population, the amplitudes of the reconstructed G_{NaTW} and of G_{NaP} were measured both at the peak [$G_{(max)}$] and at a voltage point positive by 20 mV to that of the peak [$G_{(+20)}$]. The average ratios $G_{NaTW(+20)}/G_{NaTW(max)}$ and $G_{NaP(+20)}/G_{NaP(max)}$ were 0.076 ± 0.057 ($n = 8$) and 0.715 ± 0.102 ($n = 12$), respectively ($P < 5 \times 10^{-12}$). In addition, in those neurons in which both

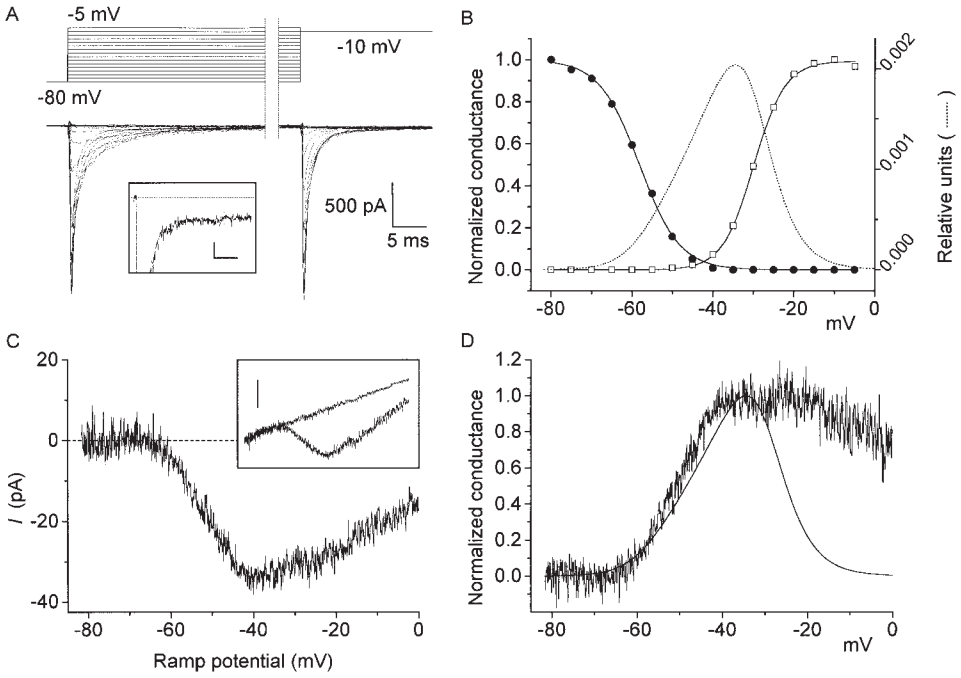

Figure 2. The I_{NaP} expressed by EC layer II principal neurons is largely not accounted for by a classical Hodgkin-Huxley window current. (A) Voltage protocols used to study the voltage dependence of activation and steady state inactivation of the fast Na^+ current (I_{NaT}) (A1), and leak-subtracted currents recorded in an exemplary acutely isolated cell (A2; cell L7719). The duration of the inactivating prepulse was 120 ms. (Inset) The current recorded at −30 mV is expanded in amplitude to highlight the presence of a persistent current (calibration bars: 20 pA, 25 ms). (B) Plots of the voltage dependence of activation (□) and steady state inactivation (●) of I_{NaT} in the same cell as in A. Na^+ conductances (G_{NaT}s) were derived from peak I_{NaT} amplitudes by applying the extended Ohm equation (materials and methods). G_{NaT} plots were normalized for the maximal values and fitted with single Boltzmann functions (continuous lines). Fitting parameters were: $V_{1/2} = -58.2$ mV, $k = 5.0$ mV (steady state inactivation); $V_{1/2} = -29.9$ mV, $k = -3.9$ mV (activation). The predicted window conductance, G_{NaTW} (results), is also shown (dotted line: note the different amplitude scale, shown on the right axis). (C) Currents evoked by a slow voltage ramp (50 mV/s) in the same cell as in A and B, before and after the application of 1 μM TTx (inset; calibration bar: 20 pA), and TTx-subtracted I_{NaP} (main panel). (D) The voltage dependence of the conductance (G_{NaP}) underlying the I_{NaP} shown in C is compared with that of the G_{NaTW} reconstructed in the same cell. Both conductances have been normalized to the maximal values.

I_{NaT} and I_{NaP} were quantified, the size of the predicted I_{NaTW} was much smaller than that of the observed I_{NaP} (see Table I). These data clearly indicate that by far most of the I_{NaP} expressed by EC layer II neurons is not a classical I_{NaTW}, similar to what has been previously observed in hippocampal neurons (French et al., 1990).

I_{NaP} Inactivates in a Time- and Voltage-dependent Manner

Whereas a depolarization-activated conductance, once maximally recruited, would be expected to maintain a steady value at more positive voltage levels, G_{NaP}, as mentioned above, consistently showed some degree of decline from its maximum. A possible explanation for this observation is the existence of a time-dependent inactivation of G_{NaP} acting during the ramp (Fleidervish and Gutnick, 1996). Under this hypothesis, G_{NaP} should inactivate more when elicited with increasingly slow ramps. To address this issue, we performed a series of experiments in which the amplitude of the I_{NaP}s evoked by voltage ramps was analyzed as a function of the ramp slope. Fig. 3 A shows the protocols applied and the TTx-subtracted currents thereby obtained in a representative in situ neuron. I_{NaP} amplitude appeared to markedly depend on the depolarization rate. The average, normalized I_{NaP} amplitude measured at the peak of the I–V function was then plotted as a function of the inverse of the ramp slope, a quantity directly related to ramp duration (Fig. 3 B) ($n = 12$). The resulting plot demonstrated a biexponential decay, with a fast "slope constant" and an ~15-fold slower one. These data strongly suggest that at least two kinetic components exist in I_{NaP}, each characterized by a different inactivation rate. The ratio between the two slope constants and that between their relative amplitude coefficients were such that, with 50-mV/s ramps, >96% of the ensuing I_{NaP}'s peak amplitude was accounted for by the slow component. Since we were interested in the slowest Na^+-current components, which more closely approach the notion of "persistent" Na^+ current, we decided to employ 50-mV/s ramps in the rest of our study so as to maintain the peak value of "true" I_{NaP}s relatively unaffected by time-dependent inactivation, while ruling out most of the "intermediate" kinetic components. Moreover, our observations confirmed the validity of applying 50-mV/s ramps for obtaining data on I_{NaP} voltage dependence of activation (see previous paragraphs).

The above data clearly pointed to the existence of a time- and voltage-dependent inactivation of I_{NaP}. However, inactivation properties of voltage-dependent channels have been shown to be possibly affected by the composition of intracellular milieu, and in particular by intracellular nonphysiological halogenic anions (Chandler and Meves, 1970; Arispe et al., 1984; Kay et al.,

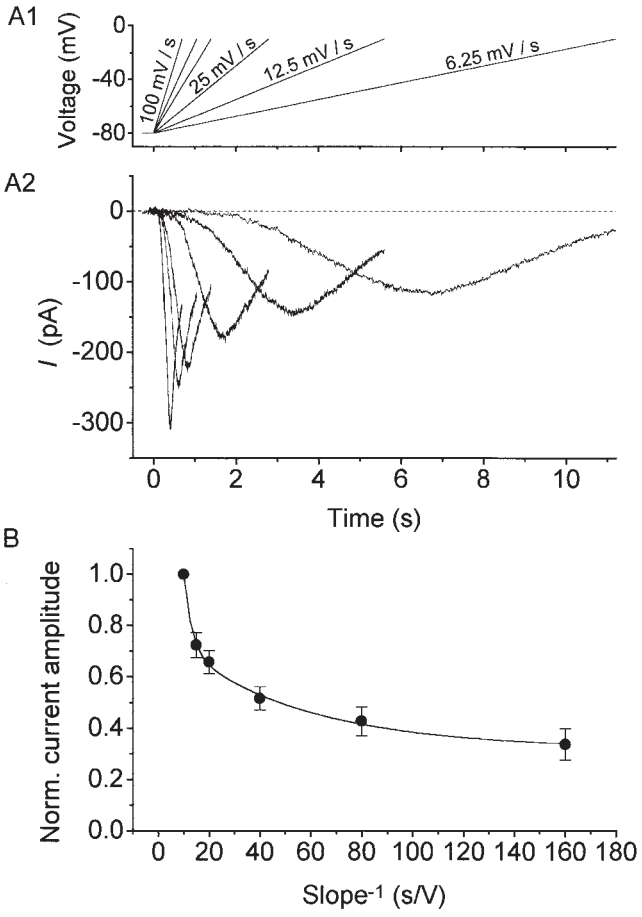

Figure 3. I_{NaP} looks different, depending on the slope of the ramp applied to elicit it. (A) Voltage ramps exploring the −80/+20-mV voltage range with different depolarization speeds (100, 66.7, 50, 25, 12.5, and 6.25 mV/s) were tested (A1), and the TTx-sensitive currents recorded in an exemplary in situ neuron (cell B7902) are depicted in A2, all over the same time scale. (B) Average, normalized I_{NaP} peak amplitude as a function of the inverse of ramp slope (n = 12; same ramp protocols as illustrated in A1). The plot could be fitted by a double exponential function [$I = A_1 \cdot \exp(-s_1/s) + A_2 \cdot \exp(-s_2/s) + C$, where s is the ramp slope and s_1 are slope constants] with $A_1 = 0.295$, $s_1 = 0.317$ V/s, $A_2 = 0.382$, $s_2 = 20.2$ mV/s (continuous line).

1986; Nisenbaum et al., 1996). Since the main anion in the intracellular solution used in our experiments was fluoride (F^-), we performed control experiments in which internal F^- was substituted with other molecules, namely sulphate (SO_4^{2-}; n = 4), and methanesulphonate ($MeSO_3^-$; n = 3). The same ramp protocols as described in the previous paragraph were applied under these ionic conditions. In no case did we observe significant differences in I_{NaP} amplitude and its ramp–slope dependence as compared with F^- experiments. In particular, peak amplitude and current density of ramp (50 mV/s)-evoked, TTx-subtracted I_{NaP}s were −155.4 ± 58.9 pA and −9.8 ± 3.6 pA/pF in SO_4^{2-} or $MeSO_3^-$ experiments (data pooled together), not significantly different from the control values reported above (P = 0.66 and 0.55, respectively). The ratio between the amplitudes of I_{NaP}s evoked by 6.25- vs. 50-mV/s ramps was 0.497 ± 0.134 in SO_4^{2-}/$MeSO_3^-$ experiments, again not significantly different from that found when using F^- (0.51 ± 0.08, n = 12, P = 0.79). These observations indicate that the above-described phenomena are indeed of physiological relevance.

We then investigated the issue of I_{NaP} inactivation in further detail by analyzing the effects of variable prepulse potentials on ramp-activated I_{NaP}s. The protocol employed is illustrated in Fig. 4 A1. 50-mV/s voltage ramps were preceded by very-long-lasting (15 s) conditioning prepulses at various voltage levels (V_{cond}). When V_{cond}s of −90 to −50 mV were used, the ramp started from the same voltage level as V_{cond} itself, rather than from a fixed, negative voltage level: in this way, the possible occurrence of recovery from inactivation during the initial part of the ramp was avoided. At more positive V_{cond}s, the ramp started from −50 mV, so as to preserve the voltage region of I_{NaP} peak. Currents recorded with the above protocol in a representative in situ neuron are shown in Fig. 4 A2. I_{NaP} peak amplitude turned out to markedly depend on the conditioning potential. Average, normalized current traces obtained from seven in situ neurons are depicted in Fig. 4 B1. It can be observed that voltage-dependent steady state inactivation of I_{NaP} was nearly complete at about −20 mV. The average plot of I_{NaP}'s voltage dependence of inactivation (Fig. 4 B2) could be fitted by a single Boltzmann function, with $V_{1/2}$ at about −49 mV and a slope factor, k, of ∼10 mV. In addition, we also constructed an activation plot from the average I_{NaP} derived from the same neuron pool, and fitted it with a single Boltzmann function (Fig. 4 B2). Note that, importantly, G_{NaP} activation and steady state inactivation functions overlapped over a wide voltage range. Due to this phenomenon, a significant window conductance (G_{NaPW}) is expected to arise from G_{NaP}. The predicted voltage dependence of G_{NaPW} is depicted in Fig. 4 B2 (dotted line), and will be compared with relevant experimental data later on in the paper.

Time Dependence of I_{NaP} Inactivation and Recovery from Inactivation

The kinetic properties of I_{NaP} voltage-dependent inactivation were then further characterized. Time dependence of inactivation was first analyzed by means of prepulse-ramp protocols (Fig. 5 B); the voltage ramp eliciting I_{NaP} was preceded by a prepulse at various voltage levels (from −60 to −20 mV), which was made to vary in duration from 0 to up to 20 s. Currents recorded in response to such a protocol in a representative in situ neuron are shown in Fig. 5 A. Average, normalized peak-current amplitudes were used for constructing plots of

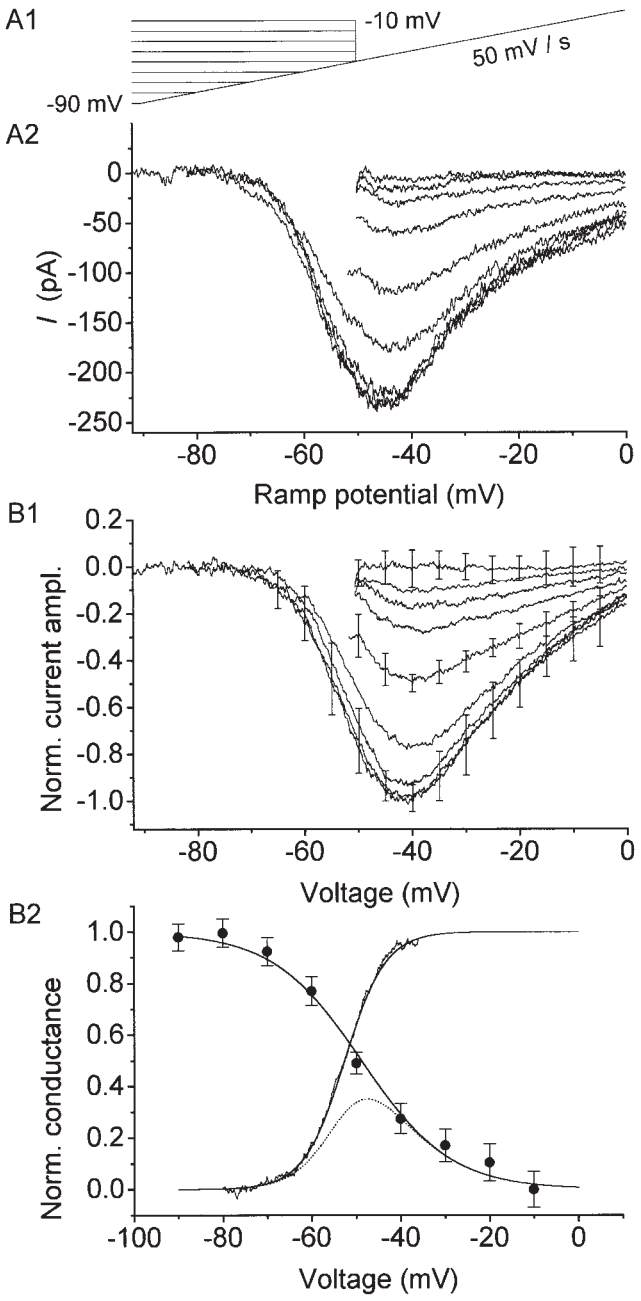

Figure 4. Voltage dependence of inactivation of I_{NaP}. (A) Voltage protocol used for the study of I_{NaP} voltage dependence of inactivation (A1), and TTx-subtracted currents recorded in an exemplary in situ neuron (A2; cell D7808). The conditioning prepulses preceding each ramp varied from −90 to −10 mV in 10-mV steps, and their duration was 15 s. Note that here, as well as in all of the voltage-clamp protocols applied in whole-cell experiments, each conditioning prepulse/ramp cycle was preceded by a 15-s period at −80 mV so as to allow recovery from the inactivation developed during the foregoing cycle (materials and methods). (B) Average currents and steady state inactivation function from seven cells. (B1) Average, normalized currents. The currents evoked in each cell as shown in A were divided by the maximal peak-current value observed in the same cell; the traces were then averaged among cells and further normalized to the maximal peak value thus obtained. Standard deviations are also shown at 5-mV intervals in the traces preceded by conditioning prepulses at −90, −50 and −10 mV. (B2) Average steady state inactivation plot (●). The amplitudes of the currents evoked as shown in A were measured at the ramp potential of −40 mV. The values thus obtained were divided by the maximal value observed in each cell, averaged among cells, and plotted as a function of the conditioning prepulse potential. The inactivation plot was best-fitted by a single Boltzmann function, with $V_{1/2} = -48.8$ mV and $k = 10.0$ mV. An average activation plot was also constructed by deriving the normalized conductance (materials and methods) from the average, normalized current obtained from the same cells (B1; prepulse potential = −90 mV), and best-fitted with a single Boltzmann function, with $V_{1/2} = -52.6$ mV and $k = -4.6$ mV. Each plot-fitting pair was further normalized to the value of the fitting-function amplitude coefficient. The dotted line represents the product of the two fitting functions, corresponding to the predicted voltage dependence of the resulting window conductance (G_{NaPW}).

time dependence of inactivation, each one referring to a specific conditioning potential (Fig. 5 C). These plots could be best fitted with single exponential functions; the time constants were slow and ranged from ~6.8 to ~2.6 s, depending on the conditioning potential.

The time course of I_{NaP} recovery from inactivation was also investigated. The voltage protocols applied (Fig. 6 B) consisted of a first 10-s prepulse at −30 mV that substantially inactivated I_{NaP}, followed by a second prepulse at −90 or −80 mV of variable duration (from 0 to 10 s), and by the standard voltage ramp. Currents recorded in response to such a protocol in a representative in situ neuron are shown in Fig. 6 A. Average, normalized peak-current amplitudes were used for constructing plots of time dependence of recovery from inactivation, for both recovery potentials (Fig. 6 C). These plots could be best fitted with single exponential functions, with time constants of ~5.2 (−80 mV), and 4.7 s (−90 mV).

A Major, Persistent Window Current Is Generated as a Consequence of G_{NaP} Gating Properties

As mentioned above and illustrated in Fig. 4 B2, the wide overlapping of I_{NaP} activation and steady state inactivation curves is expected to result in a prominent window current (I_{NaPW}) distinct from the classical window current (I_{NaTW}) predicted on the basis of the gating properties of the fast, transient Na^+ conductance. To test this prediction, voltage protocols consisting of very-long-lasting depolarizing pulses were applied to in situ neurons so as to try to uncover steady current components in I_{NaP}. Fig. 7 A1 shows average, TTx-subtracted Na^+ currents obtained from five neurons in response to 15-s voltage steps at −60 to −10 mV. After an initial phase displaying fast and intermediate-speed decay components, a slower decaying current component, which was identified as the I_{NaP} under study, became evident. When the last 14 s of the current trace were considered, the decay phase of I_{NaP} could be best fitted by a

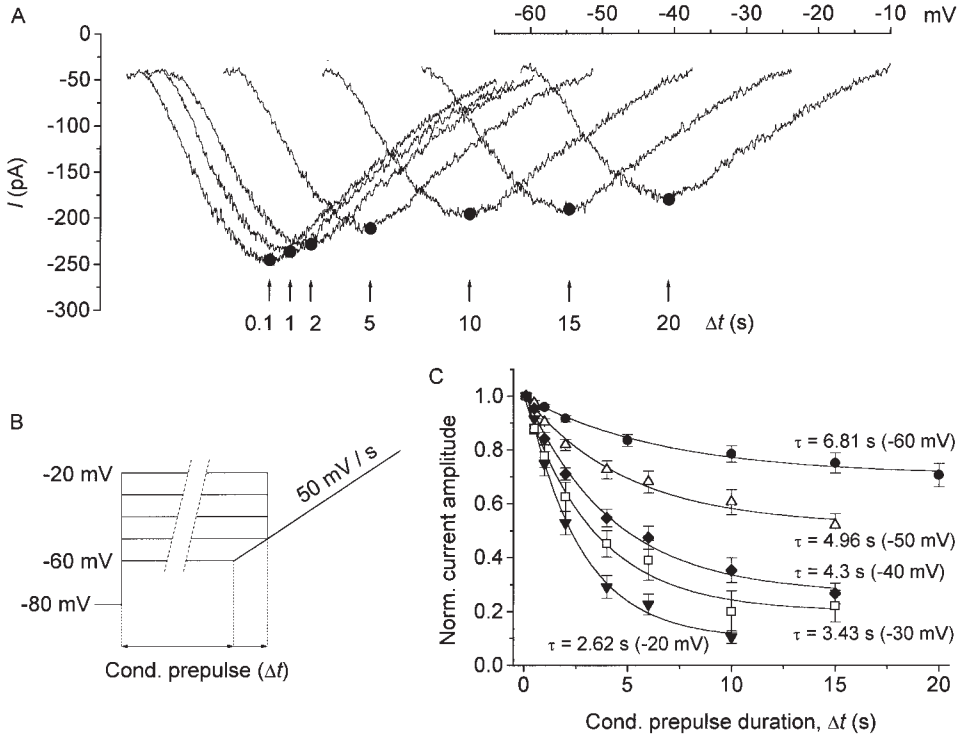

Figure 5. Time dependence of inactivation of I_{NaP}. The voltage protocols applied are shown in B. A shows TTx-sensitive currents evoked with the protocol shown in B in a representative in situ neuron (cell B7808) (prepulse potential = −60 mV). Individual currents have been staggered along the x axis by intervals proportional to the duration of the inactivating (conditioning) prepulse (Δ*t*, each indicated below the traces). The actual x (voltage) scale is indicated, for the last trace only (top right). (C) Average, normalized amplitudes of I_{NaP} as a function of depolarizing prepulse duration (mean ± SEM, n = 6–12). Each point family refers to a single prepulse voltage level. Single-exponential best fittings are also shown (continuous lines), along with time-constant (τ) values.

single exponential function, with voltage-dependent time constants very similar to those determined for the time-dependent inactivation of I_{NaP} revealed by ramp protocols (see above). In addition to the decaying component, fittings returned a steady (offset) component (I_{ss}) whose amplitude also displayed a marked voltage dependence. When plotted as a function of test potential (Fig. 7 B), the normalized I_{ss} amplitude closely par-

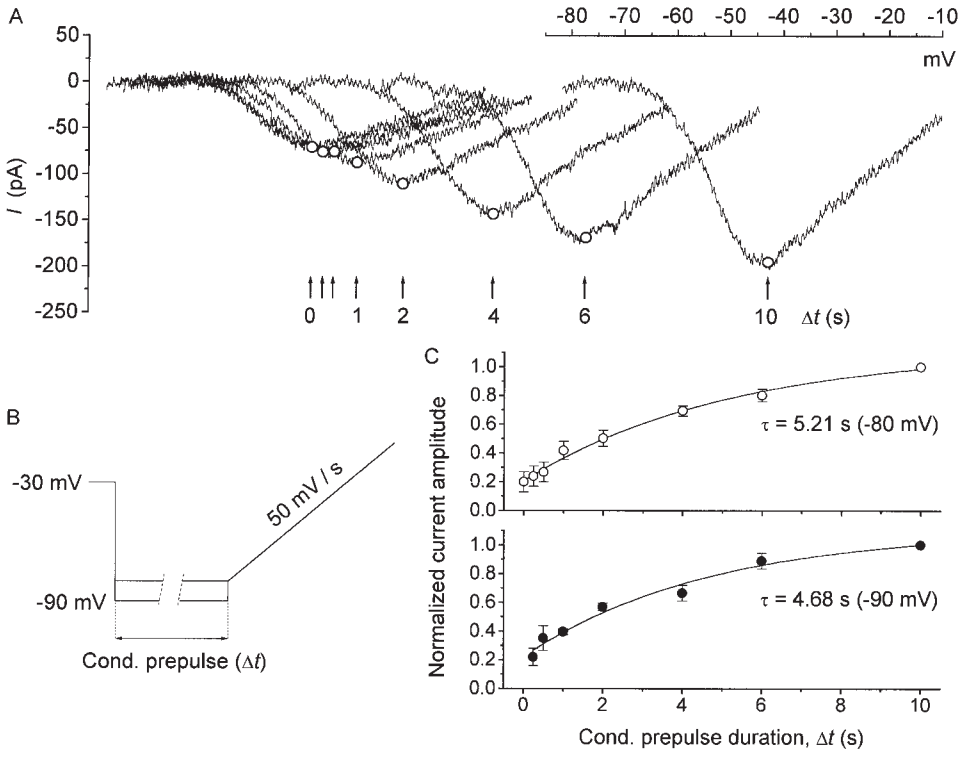

Figure 6. Time dependence of recovery from inactivation of I_{NaP}. The voltage protocols applied are shown in B. The duration of the inactivating prepulse at −30 mV was 15 s. (A) TTx-sensitive currents evoked with the protocol (B) in a representative in situ neuron (cell K7805; recovery potential = −80 mV). Individual currents have been staggered along the x axis by intervals proportional to the duration of the recovery (conditioning) prepulse (Δ*t*, each indicated below the traces). The actual x (voltage) scale is indicated, for the last trace only (top right). (C) Average, normalized amplitudes of I_{NaP} as a function of recovery-prepulse duration (means ± SEM, n = 3–8). The recovery potential was −80 (top) or −90 (bottom) mV. Single-exponential best fittings are also shown (continuous lines), along with time-constant (τ) values.

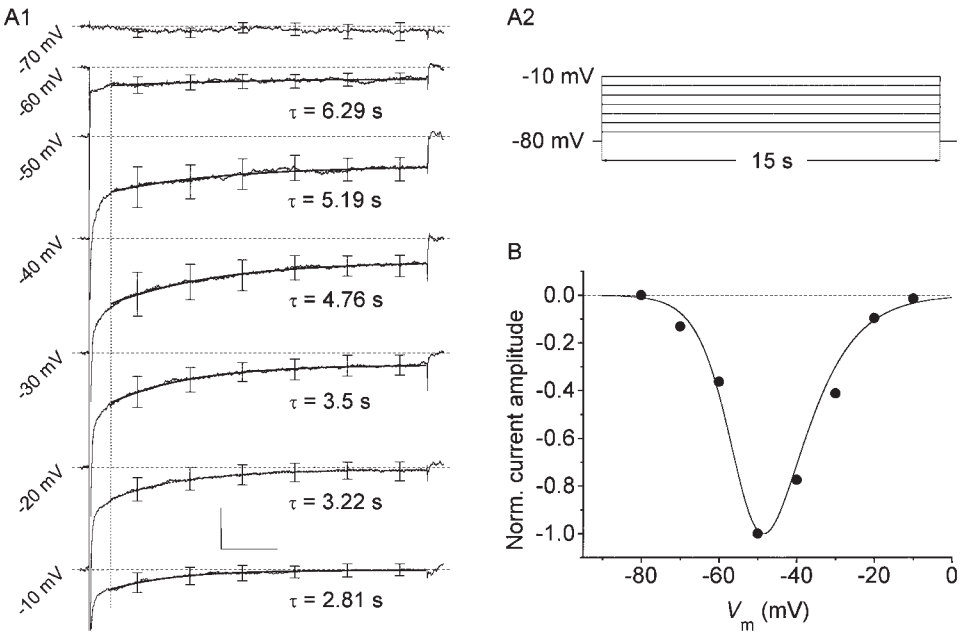

Figure 7. I_{NaP} inactivation during long-lasting depolarizing voltage steps. (A) Averaged, TTx-subtracted currents (A1) from five in situ neurons as obtained in response to 15-s voltage steps to the test potentials indicated on the left. The voltage protocol applied is shown in A2. Standard deviations for some points, single-exponential best fittings of the decay phases (enhanced lines), and time-constant (τ) values are also shown; the starting point of the fitted part of the traces is indicated by the vertical, dashed line. Scale bars: 50 pA, 2.5 s. (B) The amplitude of the noninactivating ("offset") component of average I_{NaP} (●), measured at the different test potentials, is compared with the predicted window current arising from the gating properties of I_{NaP} (I_{NaPW}, continuous line). The I_{NaPW} shown has been derived from the G_{NaPW} depicted in Fig. 4 B2 (dotted line).

alleled that of the expected I_{NaPW}. Therefore, a steady current component of I_{NaP} can be directly demonstrated whose voltage-dependent behavior fits that predicted for the time-independent I_{NaPW}.

On the basis of the above data, we then estimated the relative contribution of I_{NaPW} and I_{NaTW} to the total, noninactivating Na^+ current generated by EC layer II cells in a subthreshold region of membrane voltages, where it is known to sustain theta-like membrane-potential oscillations lasting for indefinitely long periods (Alonso and Llinás, 1989; Alonso and Klink, 1993; Klink and Alonso, 1993). Our measurements indicate that at −50 mV, a level close to that at which the maximal amplitude of subthreshold oscillations is observed (Alonso and Klink, 1993), <20% of the total, persistent Na^+ current is accounted for by I_{NaTW}, whereas the remaining part must derive from the window current generated by the true I_{NaP} (Table I).

Modeling of I_{NaP} Slow Inactivation

To further clarify the basis of the experimentally observed decline in G_{NaP} at positive potentials (Fig. 2 D), a theoretical reconstruction of the biophysical properties of I_{NaP} inactivation was carried out. A simple Hodgkin-Huxley model, considering a single inactivation gate switching between two energy states, was considered in order to give account for the monoexponential time course of I_{NaP} decay and recovery from inactivation. This reconstruction was merely phenomenological and was given no mechanistic meaning since single-channel data clearly indicated different features of the underly-

TABLE I

Absolute and Relative Amplitudes of Persistent and Window Na^+ Currents

Voltage	I_{NaTW}	I_{NaP}	I_{NaPW}	I_{NaTW}/I_{NaP}	I_{NaTW}/I_{NaPW}	
mV	*pA*	*pA*	*pA*			*n*
−50	−3.4 ± 1.3	−58.1 ± 25.0	−30.8 ± 13.2	0.071 ± 0.051	0.133 ± 0.097	5
−40	−5.2 ± 2.0	−80.6 ± 38.4	−23.6 ± 11.2	0.086 ± 0.075	0.293 ± 0.256	5

Absolute and relative amplitudes of persistent and window Na^+ currents. The window currents resulting from the gating properties of both the transient Na^+ conductance, G_{NaT} (I_{NaTW}) and the persistent Na^+ conductance, G_{NaP} (I_{NaPW}) were derived according to the following formulas: $I_{NaTW}(V) = G_{NaT(max)} \cdot (V - V_{Na}) \cdot m_\infty(V) \cdot h_\infty(V)$, where $m_\infty(V)$ and $h_\infty(V)$ values were taken from the fitting functions of G_{NaT} activation and steady state inactivation plots determined in each cell; $I_{NaPW}(V) = I_{NaP}(V) \cdot h_\infty(V)$, where $h_\infty(V)$ values were taken from the fitting function of the average G_{NaP} steady state inactivation curve (see Fig. 4 B2). Measurements are from five acutely dissociated cells in which both well-clamped I_{NaT}s and sizable I_{NaP}s were recorded. Data are mean ± SD.

ing elementary events (see below). The time constants of I_{NaP} inactivation and recovery from inactivation and the data on voltage dependence of I_{NaP} steady state inactivation were processed to derive numerical values for the rate constants of the inactivation-gate transitions, as explained in materials and methods. Fig. 8 B shows the voltage dependence of the values thus obtained for the two rate constants, α and β. The plots were then best fitted with the empirical function, α (or β) = $(a \cdot V_m + b)/\{1 - \exp[(V_m + b/a)/k]\}$, where V_m is the membrane voltage. The numerical values returned by the fittings for the *a*, *b*, and *k* coefficients, in both the α and β plots, are indicated in the legend to Fig. 8. The voltage-dependence functions thus obtained for α and β were then used to derive the predicted voltage dependence of I_{NaP} inactivation-gating time constants (see materials and methods). The concordance between the reconstructed, theoretical function and the real data is shown in Fig. 8 A.

The kinetic parameters obtained in the above manner were then used to verify the possible effects of I_{NaP} slow inactivation on the results of voltage-clamp ramp protocols. Reconstructed I_{NaP}s evoked by simulated voltage ramps of variable slope are illustrated in Fig. 8 C. It is apparent that progressively reducing the depolarization rate causes a decrease in I_{NaP} peak amplitude, and the appearance of increasing discrepancies between the true I_{NaP} voltage dependence and that measured in the late part of the ramp protocol. Fig. 8 E shows the voltage dependence of G_{NaP} as obtained in response to a simulated 50 mV/s-ramp protocol: the reconstructed G_{NaP} declined at voltages positive to about −30 mV very similarly to the experimentally observed G_{NaP} (see Fig. 2 D), whereas G_{NaP} voltage dependence

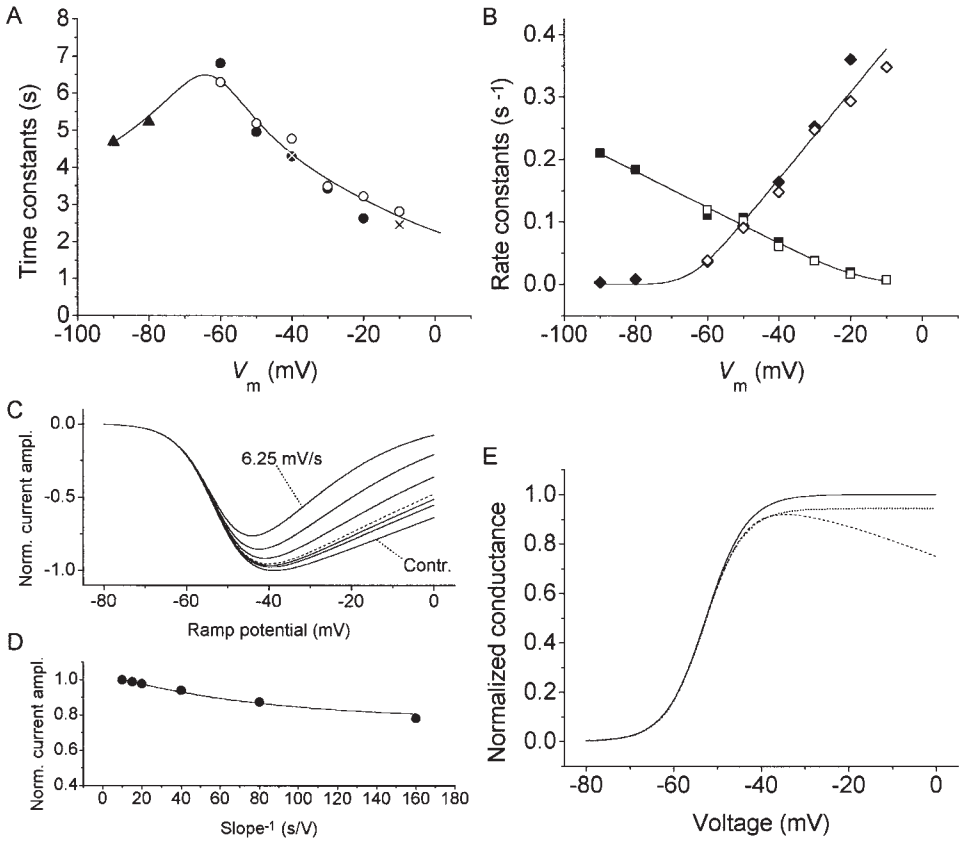

Figure 8. Modeling of I_{NaP} inactivation and of its consequences on ramp protocols. (A) Time constants of I_{NaP} inactivation (circles) and recovery from inactivation (triangles) as a function of membrane voltage. Time constants of inactivation (τ_h) determined with both ramp (●) and step (○) protocols are shown. The continuous line is the theoretical function describing $\tau_h(V)$, as obtained from the fitting functions of the voltage dependence of rate constants (see below). Crosses indicate time constants of inactivation of ensemble-average traces obtained in single-channel, cell-attached experiments (see text), here included for comparison. (B) Rate constants of the transitions of the inactivating gate, *h*, to (α) and from (β) the permissive position (see results and materials and methods for details). Values for α (squares) and β (diamonds) have been calculated, as explained in materials and methods, on the basis of time constants measured from both ramp (filled symbols) and step (empty symbols) protocols. The continuous lines represent the fitting functions (described in results) for α(V) and β(V), with $a = -2.88 \cdot 10^{-3}$ mV^{-1} s^{-1}, $b = -4.9 \cdot 10^{-2}$ s^{-1}, $k = 4.63$ mV (α); $a = 6.94 \cdot 10^{-3}$ mV^{-1} s^{-1}, $b = 0.447$ s^{-1}, $k = -2.63$ mV (β). (C) Effects of I_{NaP} inactivation on the amplitude and shape of the I_{NaP}s generated by simulated voltage-ramp protocols with different depolarization slopes. The curves shown correspond to the "ideal" (unperturbed) I_{NaP} (Contr.), and to I_{NaP}s generated by simulated voltage ramps of 100, 66.7, 50 (dashed line), 25, 12.5, and 6.25 mV/s. For describing the voltage dependence of activation of the conductance underlying I_{NaP} (G_{NaP}), the same parameters as obtained from the data of Fig. 4 B2 were used in these simulations. (D) Dependence of I_{NaP} peak amplitude on the inverse of voltage-ramp slope in simulated experiments. The data points shown were derived from the same current traces depicted in C. The plot has been fitted with a single exponential function (continuous line), with $A = 0.23$, $\varsigma = 12.8$ mV/s. (E) The voltage dependence of G_{NaP} in a simulated 50-mV/s ramp protocol (dashed line) is compared with that of the ideal (unperturbed) G_{NaP} (continuous line). The initial part (negative to −36 mV) of the same curve has also been best fitted with a single Boltzmann function (dotted line). Fitting parameters were: $V_{1/2} = -53.0$ mV, $k = -4.5$ mV.

of activation, as measured by considering only the early part of the ramp protocol, was negligibly affected. Moreover, the plot of reconstructed I_{NaP}'s peak amplitude as a function of the inverse of ramp slope (Fig. 8 D) could be fitted, with some approximation, with a single exponential function, with a slope constant (s) similar to the slow slope constant observed in experimental plots (see Fig. 3 B), and no sign of any fast, early component. The latter results further confirm the adequacy of the ramp protocol we routinely used for characterizing the biophysical properties of I_{NaP}, and in particular the slow inactivation of this current.

Finally, a simulated protocol of steady state inactivation revealed that, during a ramp preceded by a prepulse that fully inactivates I_{NaP}, a significant recovery from inactivation can occur provided that the ramp starts at sufficiently negative levels and is sufficiently slow. For instance, during a 25-mV/s ramp starting at −80 mV, 17% of the total current can recover from inactivation (not shown). By contrast, voltage protocols similar to those we employed for the study of I_{NaP} voltage-dependent inactivation (see above) determined no appreciable ramp-dependent recovery from inactivation of I_{NaP}.

Single-Channel Bases of I_{NaP} Slow Inactivation and I_{NaPW} Generation

The single-channel basis of I_{NaP} in EC layer II neurons has been described elsewhere (Magistretti et al., 1999). In that study, we found that, after membrane step depolarization, I_{NaP} is generated by early as well as late single Na^+-channel openings of much more prolonged duration and of significantly higher conductance than the usual, transient Na^+-channel openings responsible for I_{NaT} generation. Here, we report how the same persistent Na^+-channel activity also accounts for some particular biophysical properties described for macroscopic I_{NaP}, namely I_{NaP} time-dependent inactivation and I_{NaPW} generation.

Recordings from cell-attached patches in acutely isolated EC layer II neurons frequently revealed the presence of a persistent Na^+-dependent channel activity that proved to remain stable even over prolonged periods of time (tens of minutes). When very-long-lasting (20 s) depolarizing steps at −10 mV were commanded from a holding potential of −80 mV, multiple, repetitive single-channel openings were observed that tended to cluster preferentially at the beginning of the test pulse. Typical examples of this channel activity for a series of consecutive 20-s test pulses is shown in Fig. 9 A1. A detail of some prolonged, late channel openings is also provided by Fig. 9 A1, inset. Ensemble averaging of multiple traces was then carried out for each patch (Fig. 9 A2). Due to the very long overall duration of the recording cycle required for every single sweep (40 s), only a limited number of traces could be recorded in each patch (15 on average), what explains the low signal-to-noise ratio of ensemble-average traces. In all cases, however, the averaged currents showed a noticeable trend to decay towards zero, and this decay could be properly fitted by a single exponential function (Fig. 9 A2, blank trace). The time constant of average-current decay was 2.66 ± 0.52 s in six patches at −10 mV, a value that compares favorably with those found in whole-cell protocols on macroscopic I_{NaP} inactivation at the most positive voltage levels tested (see Fig. 8 A). Ensemble averaging of all of the available sweeps recorded from the same six patches returned a better signal-to-noise ratio (Fig. 9 B). The decay time constant of the resulting average current was 2.46 s, again in good agreement with the data obtained from the analysis of both individual patches and whole-cell recordings.

The open-time distribution of the single-channel activity evoked by 20-s depolarizing steps at −10 mV was then investigated. Fig. 10 A shows the open-time distribution found in the same patch as illustrated in Fig 9 A. As in this case, all plots were best fitted by double-exponential functions, with average time constants of 3.35 ± 0.86 and 21.07 ± 17.74 ms, and an average ratio of the slow vs. fast exponential-component weight ($W = A \cdot \tau$) of 0.118 ± 0.048 ($n = 6$). It seems important to point out at this time that: (a) even the faster of the two time constants exceeds by more than six times the mean open time found in classical, transient Na^+ channel openings at approximately the same test voltage level (Aldrich et al., 1983; Alzheimer et al., 1993b); yet (b) the values of both time constants were much smaller than those of the time constants of inactivation of ensemble-average currents as well as whole-cell I_{NaP}. This specific issue will be further addressed below.

Long-lasting depolarizing protocols at more negative test-voltage levels were also applied in cell-attached recordings so as to investigate the possible bases of I_{NaPW} generation. A typical example of the recordings obtained at the test voltage of −40 mV is shown in Fig. 11 A. Again, multiple, repetitive single-channel openings were observed and these were able to generate a measurable inward current in ensemble-average traces (Fig. 11 B). Note, however, that at these more negative voltage levels channel openings were more widely distributed over the entire 20-s sweeps. Consequently, at −40 mV the ensemble average-current decayed at a slower rate (with a time constant of 4.33 ms) than at −10 mV. In addition, this decay was towards a steady value (C in exponential fittings; see materials and methods) that was higher than zero and represented 25.1% of the current's total amplitude coefficient (namely $A + C$). These data are in good agreement with the whole-cell data on I_{NaP} inactivation and I_{NaPW} generation illustrated above.

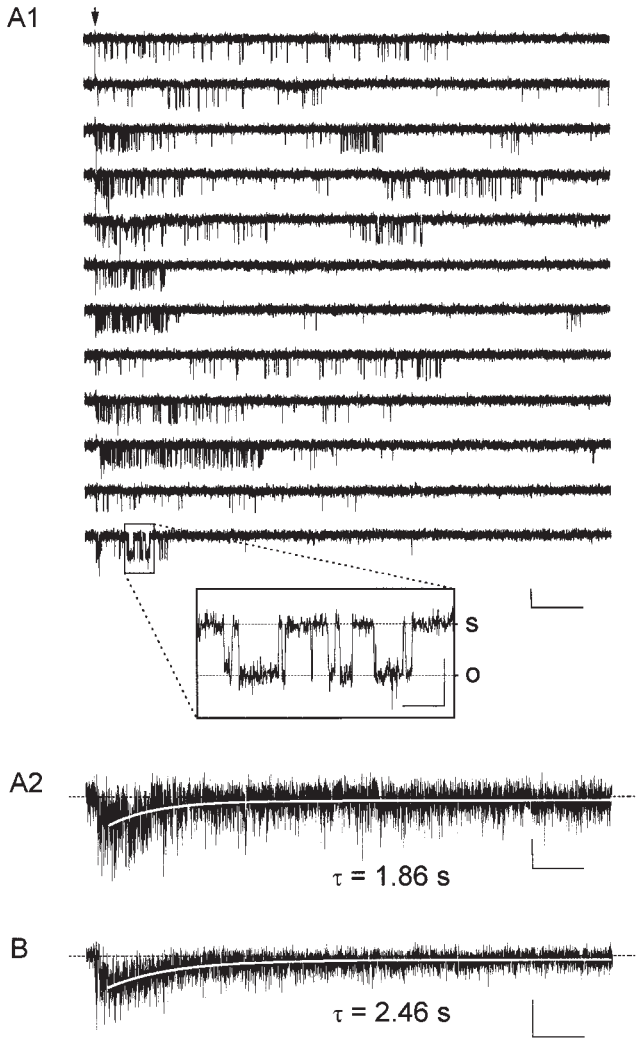

Figure 9. Single-channel basis of I_{NaP} slow inactivation. (A) Cell-attached recordings at the test potential of −10 mV in a representative patch from an acutely isolated EC layer II neuron (patch D8708). The patch was held at −80 mV, and 20-s depolarizing pulses were delivered beginning from the time point marked by the arrow. A1 shows 12 sweeps selected from an ensemble of 20 (scale bars: 1 pA, 2 s). (Inset) Detail of long-lasting single-channel openings (scale bars: 1 pA, 200 ms). The shut- (s) and open- (o) channel levels used in dwell-time analysis are marked by the horizontal, dashed lines. A2 illustrates the ensemble average of the 20 sweeps recorded from the same patch as in A1 (scale bars: 0.1 pA, 2 s). The single-exponential best fitting of the average current's decay phase (blank line) and the corresponding time-constant value are also shown; values for A and C (see materials and methods) were −83.3 and −12.4 fA, respectively. (B) Ensemble average of 86 sweeps recorded at the test potential of −10 mV, with the same experimental protocol as explained above, from six different patches (scale bars: 0.1 pA, 2 s). The single-exponential best fitting of the average current's decay phase (blank line) and the corresponding time-constant value are also shown (values for A and C were −74.4 and −11.7 fA, respectively).

They are also consistent with the idea that the same single-channel events can account for I_{NaP} as well as a steady, nondecaying Na^+-current component (namely I_{NaPW}) generated within a limited voltage window, where it represents a substantial fraction of total I_{NaP}.

Finally, the analysis of open-time distribution at −40 mV also revealed the existence of two exponential components (Fig. 10 B), with average time constants of 1.33 ± 0.14 and 6.63 ± 3.47 ms, and an average W_2/W_1 ratio of 0.069 ± 0.042 (n = 3). At this potential, therefore, the discrepancy between mean open times and time constants of inactivation of both ensemble-average currents and macroscopic I_{NaP} was even bigger than at −10 mV.

The observation that the channel mean open times are far exceeded by the time constants of ensemble-average current inactivation clearly indicates that the latter do not reflect average channel-opening lifetimes in a simple model considering two open states each undergoing one single closure process (with rate constant b) towards an absorbing state, like:

$$C \overset{a_i}{\rightarrow} O_i \overset{b_i}{\rightarrow} I_i, \qquad \text{(SCHEME I)}$$

with the index i being either 1 or 2, and with $a_i >> b_i$. Rather, alternative models considering late first openings and/or late reopenings must be taken into account. In an extreme situation, late channel openings such those of Fig. 9 A1 might all be first openings of as many distinct channels inactivating towards an absorbing state, in a model qualitatively similar to that depicted in Scheme I, but in which the kinetics of the macroscopic inactivation process would rather reflect the rate constants of the closed-to-open reactions, a_i. This interpretation, which resembles the classical Aldrich-Corey-Stevens model of the kinetics of transient Na^+ channels (Aldrich et al., 1983), seems very unlikely since, in patches containing most likely only one "persistent" channel, delayed first openings occurred very infrequently, whereas late reopenings were often observed (Magistretti et al., 1999). An alternative possibility is that the channel, once open, can reach multiple nonconductive states, one of which is virtually absorbing at positive potentials, thus causing a true channel inactivation. Under this assumption, a channel behavior such as that in Fig. 9 A1 could be accounted for by repetitive reopenings of a small number of persistent channels. The most economical kinetic scheme of such a behavior is seen in Scheme II.

$$\begin{array}{ccc} & \overset{\alpha_i}{} & \\ O_i & \rightleftharpoons & C \\ \gamma_i \downarrow & & \beta_i \\ I_i & & \end{array} \qquad \text{(SCHEME II)}$$

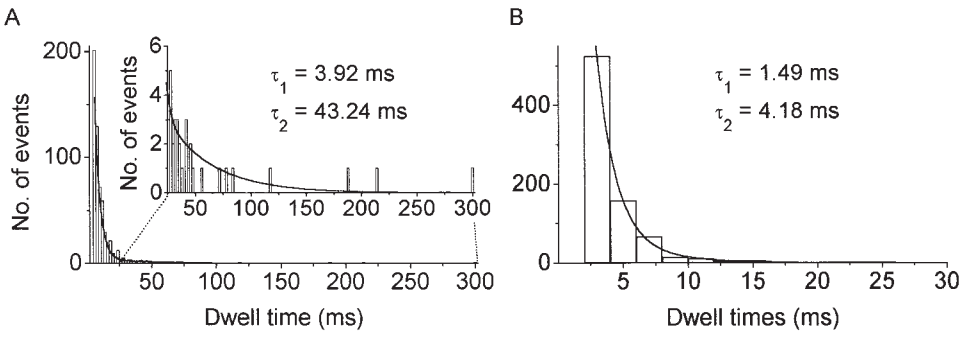

Figure 10. Frequency distribution of dwell times of "persistent" channels in the open state in long-lasting (20 s) depolarizing step protocols. (A) Open-time histogram of channel openings recorded at the test potential of −10 mV in the same patch as shown in Fig. 9 A. (Inset) Detail of the histogram's region from 25 ms upwards. A double-exponential best fitting (continuous lines) and the corresponding time-constant values are also shown; the W_2/W_1 ratio (see results for details) was 0.081. (B) Open-time histogram of channel openings recorded at the test potential of −40 mV in the same patch as shown in A. A double-exponential best fitting (continuous line) and the corresponding time-constant values are also shown; the W_2/W_1 ratio was 0.099.

A nonnegligible rate constant (δ) for the reaction $I_i \rightarrow O_i$ should also be considered for more negative voltages, at which a major I_{NaPW} is produced. The analytical derivation of relaxation time constants from rate constants (see Colquhoun and Hawkes, 1977, 1981) reveals that if $\alpha_i >> \gamma_i$, and $\gamma_1 \approx \gamma_2$ (or if only one inactivated state exists, communicating with one of the two open states), one slow time constant of ensemble-average current inactivation would be produced, which would faithfully reflect $1/\gamma$. Other possible kinetic schemes consider that an inactivated state is reached from a closed rather than a conducting state. The evaluation of the relationships between transition rate constants in such a scheme and the time constants of ensemble-average current inactivation would require the study of closed-time distribution. This could not be reliably accomplished from our data since in no patches in which slow inactivation was studied could the presence of one single channel be assumed. Despite these limitations in providing precise kinetic schemes, our data clearly demonstrate the importance of late channel (re)openings, rather than of early, very-long-lasting openings, for the generation of slow kinetic components in macroscopic I_{NaP}.

DISCUSSION

The present study provides a biophysical characterization of the I_{NaP} expressed by rat EC layer II principal neurons. The major issues we addressed deal with the mechanism of generation of I_{NaP}, the possible influence of the voltage protocols employed for the study of I_{NaP} biophysical properties, and the real degree of I_{NaP} persistence over time and specific voltage windows.

In general, the hypotheses on generation of persistent Na^+ currents consider two main possibilities: (a) I_{NaP} simply derives from an incomplete steady inactivation of transient Na^+ channels over a narrow voltage window, due to the partial superimposition of activation and steady state inactivation voltage-dependence curves of the corresponding conductance; (b) I_{NaP} is the result of channel openings that do not functionally behave according to the properties of transient Na^+ channels, but derive from a rare and atypical gating modality of the same channels (Alzheimer et al., 1993b), possibly under modulatory control by G proteins (Ma et al., 1997) or other factors, or, alternatively, from a different channel species. To discriminate between these two possibilities, it is necessary to accurately determine the properties of the window current generated by transient Na^+ channels and compare them with those of I_{NaP} present in the same cell preparation. The study of acutely dissociated EC neurons allowed us to perform careful measurements on I_{NaT}, and therefore to make reliable predictions on the resulting I_{NaTW}. The comparison between I_{NaTW} and I_{NaP} was done both on a statistical basis and, in some cases, in the same cells. Our data on the voltage dependence and amplitude of these currents indicate that I_{NaTW}, in contrast with what was reported in a previous study (Fan et al., 1994), cannot be a major source of the I_{NaP} expressed by EC principal neurons. An alternative, specialized mechanism must be implied in the generation of the large I_{NaP}s found in these neurons. An exciting possibility, already suggested elsewhere on the basis of whole-cell data (French et al., 1990), is that I_{NaP} is generated by a specialized Na^+ channel at least biophysically distinct from those generating the fast transient Na^+ current (Masukawa et al., 1991). Indeed, single-channel, patch-clamp experiments in EC layer II neuron somata indicate that while I_{NaT} is generated by a typical ~15-pS channel with fast activation and inactivation kinetics, I_{NaP} is due to an ~20-pS channel activity with a 10-mV lower threshold of activation, and a sustained, high open probability during prolonged depolarizations (Magistretti et al., 1999). The issue regarding the molecular diversity of Na^+ channels (see Ragsdale and Avoli, 1998, for recent review) expressed by EC layer II neurons is beyond the scope of the present study and will be discussed elsewhere.

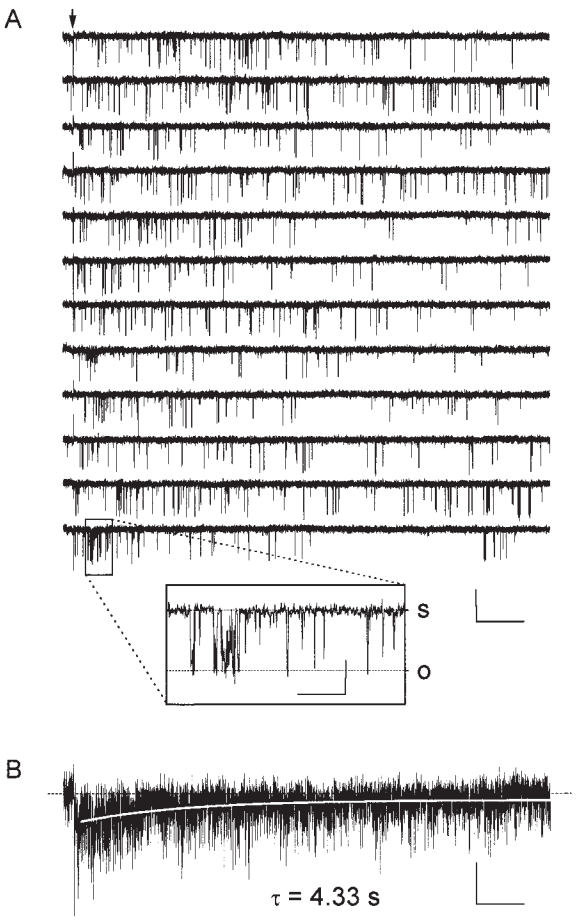

Figure 11. Single-channel basis of I_{NaPW} generation. (A) Cell-attached recordings at the test potential of −40 mV in a representative patch from an acutely isolated EC layer II neuron (patch D8617). The patch was held at −80 mV, and 20-s depolarizing pulses were delivered beginning from the time point marked by the arrow. The traces shown are 12 consecutive sweeps (scale bars: 2 pA, 2 s). (Inset) Time expansion of some single-channel openings (scale bars: 2 pA, 200 ms). The shut- (s) and open- (o) channel levels used in dwell-time analysis are remarked by the horizontal dashed lines. (B) Ensemble average of 33 sweeps recorded at the test potential of −40 mV, with the same experimental protocol as explained above, from three different patches (scale bars: 0.1 pA, 2 s). The single-exponential best fitting of the average current's decay phase (blank line) and the corresponding time-constant value are also shown; values for A and C (see materials and methods) were −51.7 and −17.3 fA, respectively.

Another interesting issue raised by our data relates to the definition itself of I_{NaP}. Due to their practicality, ramp protocols are the most widely used means for eliciting and isolating I_{NaP}. However, the employment of such protocols presupposes that they can adequately reproduce the voltage dependence of I_{NaP} without significantly recruiting any other kinetically different (i.e., faster-decaying) Na^+-current component. This is often implicitly assumed rather than demonstrated. Moreover, the notion of "slow voltage ramp" suitable for I_{NaP} activation varies considerably among different experimental works (Alzheimer et al., 1993a; Uteshev et al., 1995; Cepeda et al., 1995; Pennartz et al., 1997; Parri and Crunelli, 1998; Cummins et al., 1998). The experiments we carried out by running voltage ramps of variable slopes clearly indicate that the amplitude of the ensuing I_{NaP} strictly depends on the depolarization rate applied. Our data show how, when ramps of progressively decreasing slopes (from 100 to 6.25 mV/s) are commanded, I_{NaP} amplitude decreases in a roughly biexponential fashion. The existence of a faster exponential component may be due to the presence of Na^+-current components kinetically intermediate between classical, "fast" Na^+ currents and the persistent Na^+ current. These intermediate kinetic components were easily observed in our step-protocol recordings (see Figs. 1 A and 7 A1), and their properties in EC layer II stellate cells will be described in detail elsewhere. The measurements on I_{NaP}s evoked with "slow" voltage ramps may therefore be contaminated by the superimposition of such current components, unless the commanded ramp is slow enough.

Moreover, our data show that, importantly, the process of I_{NaP} slow inactivation is a potential source of distortions in the measurements of I_{NaP} biophysical parameters (amplitude, voltage dependence of activation, reversal) when this current is elicited by voltage ramps. All these considerations point to the importance of accurately choosing the voltage protocol applied for the study of I_{NaP} in each specific experimental situation. We propose that some previously reported, atypical biophysical features of I_{NaP}, particularly regarding its nonsigmoidal voltage dependence of activation (Brown et al., 1994), are the result of the interaction between multiple Na^+-current slow decay components and the ramp protocols employed. In our study, the ramp protocols routinely used were chosen so as to minimize both the possible contribution of intermediate-kinetics Na^+ current components and the effects of voltage- and time-dependent inactivation of I_{NaP}.

The inactivation properties of what, according to our operative definition, can be considered as I_{NaP} have been characterized in detail in our study. Our experiments indicate that, in our preparation, the steady state inactivation of the conductance underlying I_{NaP} (G_{NaP}) (a) has a voltage dependence that extends over a wide voltage window, and (b) reaches a nearly complete level at −20 to −10 mV. The former of these features, together with the relative position of the G_{NaP} activation curve along the voltage axis, is expected to give rise to a major, time-independent, "window" current over a limited voltage range. This window current (I_{NaPW}), clearly different from that arising from the voltage-dependence properties of the transient Na^+ conductance (I_{NaTW}), could also be directly demonstrated both as nonzero

baselines at the beginning of ramp protocols on voltage dependence of inactivation (see Fig. 4), and as offsets, or pedestals, in exponentially decaying I_{NaP}s elicited by long-lasting voltage steps (Fig. 7). The peak of the observed I_{NaPW} occurred at voltage levels very close to those at which I_{NaP}-dependent, theta-like subthreshold membrane-potential oscillations are generated by EC stellate cells (Alonso and Llinás, 1989; Alonso and Klink, 1993; Klink and Alonso, 1993; van der Linden and Lopes da Silva, 1998). Our data indicate that the contribution of I_{NaPW} to the total persistent Na^+ current over the voltage range of subthreshold-oscillation generation must be substantial, since the peak I_{NaPW} amplitude was estimated to exceed that of the predicted I_{NaTW} by more than four times. Since the subthreshold oscillations generated by the stellate cells can last indefinitely, our observations also imply that only a fraction of the total I_{NaP}, namely I_{NaPW} itself, is sufficient for sustaining them.

I_{NaP} slow inactivation and recovery from inactivation were found to occur with voltage-dependent time constants in the order of a few seconds. We worked out an analytical reconstruction of the kinetics of these processes which, if introduced into suitable neuronal models, should allow us to make predictions on the effects of slow voltage-dependent inactivation on I_{NaP} modulation of membrane-voltage events. We demonstrated that I_{NaP} inactivation can considerably affect the apparent current maximal amplitude during the delivery of slow depolarizing ramps. Therefore, it is conceivable that the recruitment of I_{NaP} and its impact onto membrane-voltage dynamics can be significantly influenced by the speed of membrane depolarization. For instance, the ability of I_{NaP} to bring the membrane potential towards threshold for action-potential firing may be expected to be higher in response to a step depolarizing current injection than to slower or sustained depolarizations. This is consistent with the role of I_{NaP}, demonstrated in various central nervous system neurons (Jahnsen and Llinás, 1984; Franceschetti et al., 1995; Parri and Crunelli, 1998) including EC stellate cells (Alonso and Klink, 1993; Klink and Alonso, 1993) in promoting transient low-threshold spikes and sustaining phasic firing in response to fast depolarizations. On the other hand, I_{NaP} inactivation, which we found to be eventually complete above a physiologically interesting range of membrane potentials, may have an important role in limiting detrimental Na^+ influx during pathological conditions such as seizures and ischaemia (see also Taylor and Meldrum, 1995).

The question can then be raised whether the biophysical properties we describe here for the I_{NaP} expressed by EC stellate cells represent a general feature of this current in various neuronal populations. Slow time-dependent inactivation of I_{NaP} has been previously reported in neocortical pyramidal neurons (Fleidervish and Gutnick, 1996), although in that case the voltage dependence of the process was not investigated in detail, whereas a nondecaying "offset" I_{NaP} component corresponding to ~30% of the total was found in experiments on time dependence of inactivation even after inactivating prepulses at +20 mV. This is in contrast with our finding of a virtually complete inactivation at approximately −20/−10 mV. The discrepancy may imply the existence of interesting functional differences among I_{NaP}s expressed by different neuronal populations, which encourages further studies in other cell systems; alternatively, it may be the consequence of the inactivation protocol employed in Fleidervish and Gutnick (1996), in which the depolarizing ramp after the inactivating prepulse started from a fixed, negative voltage level (−80 mV): this may allow some degree of recovery from inactivation during the early phase of the ramp, as also suggested by the output of our modeling study (results).

Finally, the present study provides an insight into the fine mechanisms underlying the complex biophysical features displayed by I_{NaP}. Our previous work has already clarified the nature and elementary properties of the single-channel events responsible for I_{NaP} generation in EC principal neurons (Magistretti et al., 1999). The data we report here clearly point to the importance of late Na^+-channel (re)openings, many times longer in duration than those generating classical, transient I_{NaT} in central neurons, for determining the behavior of slow kinetic components of macroscopic I_{NaP}. Late Na^+-channel (re)openings have already been identified as a possible source of I_{NaP} in neocortical neurons (Alzheimer et al., 1993b) and ventricular myocytes (Ju et al., 1994), but those we observed were comparatively much longer-lived. The slow inactivation of whole-cell I_{NaP} we characterized was paralleled by that of ensemble-average traces from single-channel, cell-attached recordings. In turn, the latter appeared to be the consequence of the slow delivery of channels to an inactivated state. This can be the consequence of either late first openings or, much more probably, low-rate transitions from open states that are more likely to switch to a close, re-recruitable state, or vice versa. The inactivated state was nearly absorbing at −10 mV, but not at −40 mV, where the existence of a major window current generated by the voltage-dependent properties of G_{NaP} had been predicted and demonstrated (see above). Again, whole-cell I_{NaPW} had its single-channel correlate in late, repetitive openings able to generate measurable net inward currents after as long as 20 s of membrane depolarization.

In conclusion, the I_{NaP} expressed by EC layer II principal neurons is a prominent current operating in a subthreshold range of membrane potentials, most of which is generated by a process independent of the

classical gating behavior of the transient Na^+ conductance. It also displays complex and previously nonrecognized biophysical characteristics that appear to be tailored to the specific role this current is known to play in the generation of the sub- and near-threshold membrane-potential events typical of the same neurons. The concept of "persistent Na^+ current" may turn out to be susceptible to some critical revision also in other experimental situations, with reference to both the existence of multiple and heterogeneous functional components, and the expression of kinetic and voltage-dependence properties that might influence their impact onto neuronal function in previously unforeseen ways.

J. Magistretti thanks the Human Frontier Science Program Organization (HFSPO), the Istituto Nazionale Neurologico "Carlo Besta," and Dr. Marco de Curtis for support.

This work has been funded by grants from the Medical Research Council of Canada, HFSPO, and the North Atlantic Treaty Organization to A. Alonso.

Submitted: 2 June 1999 Revised: 4 August 1999 Accepted: 9 August 1999

REFERENCES

Adey, W.R., C.W. Dunlop, and C.E. Hendrix. 1960. Hippocampal slow waves: distribution and phase relationships in the course of approach learning. *Arch. Neurol.* 3:74–90.

Adey, W.R., S. Sunderland, and C.W. Dunlop. 1957. The entorhinal area: electrophysiological studies of its interrelations with rhinencephalic structures and the brainstem. *Electroencephalogr. Clin. Neurophysiol.* 9:309–324.

Aldrich, R.W., D.P. Corey, and C.F. Stevens. 1983. A reinterpretation of mammalian sodium channel gating based on single channel recording. *Nature.* 306:436–441.

Alonso, A., M. de Curtis, and R. Llinás. 1990. Postsynaptic Hebbian and non-Hebbian long-term potentiation of synaptic efficacy in the cortex in slices and in the isolated adult guinea pig brain. *Proc. Natl. Acad. Sci. USA.* 87:9280–9284.

Alonso, A., and E. García-Austt. 1987a. Neuronal sources of theta rhythm in the entorhinal cortex of the rat. I. Laminar distribution of theta field potentials. *Exp. Brain Res.* 67:493–501.

Alonso, A., and E. García-Austt. 1987b. Neuronal sources of theta rhythm in the entorhinal cortex of the rat. II. Phase relations between unit discharges and theta field potentials. *Exp. Brain Res.* 67:502–509.

Alonso, A., and R. Klink. 1993. Differential electroresponsiveness of stellate and pyramidal-like cells of medial entorhinal cortex layer II. *J. Neurophysiol.* 70:128–143.

Alonso, A., and R.R. Llinás. 1989. Subthreshold Na^+-dependent theta-like rhythmicity in stellate cells of entorhinal cortex layer II. *Nature.* 342:175–177.

Alzheimer, C., P.C. Schwindt, and W.E. Crill. 1993a. Postnatal development of a persistent Na^+ current in pyramidal neurons from rat sensorimotor cortex. *J. Neurophysiol.* 69:290–292.

Alzheimer, C., P.C. Schwindt, and W.E. Crill. 1993b. Modal gating of Na^+ channels as a mechanism of persistent Na^+ current in pyramidal neurons from rat and cat sensorimotor cortex. *J. Neurosci.* 13:660–673.

Amitai, Y. 1994. Membrane potential oscillations underlying firing patterns in neocortical neurons. *Neuroscience.* 63:151–161.

Arispe, N.J., J.A. Argibay, and L.V. Rojas. 1984. Sodium currents in skeletal muscle fibres from the toad *Bufo marinus. Q. J. Exp. Physiol.* 69:507–519.

Baker, M.D., and H. Bostock. 1997. Low-threshold, persistent sodium current in rat large dorsal root ganglion neurons in culture. *J. Neurophysiol.* 77:1503–1513.

Brown, A.M., P.C. Schwindt, and W.E. Crill. 1994. Different voltage dependence of transient and persistent Na^+ currents is compatible with modal-gating hypothesis for sodium channels. *J. Neurophysiol.* 71:2562–2565.

Buzsáki, G. 1996. The hippocampal-neocortical dialogue. *Cereb. Cortex.* 6:81–92.

Cepeda, C., S.H. Chandler, L.W. Shumate, and M.S. Levine. 1995. Persistent Na1 conductance in medium-sized neostriatal neurons: characterization using infrared videomicroscopy and whole cell patch-clamp recordings. *J. Neurophysiol.* 74:1343–1348.

Chandler, W.K., and H. Meves. 1970. Sodium and potassium currents in squid axons perfused with fluoride solutions. *J. Physiol.* 211:623–652.

Chao, T.I., and C. Alzheimer. 1995. Do neurons from rat neostriatum express both a TTX-sensitive and a TTX-insensitive slow Na^+ current? *J. Neurophysiol.* 74:934–941.

Colquhoun, D., and A.G. Hawkes. 1977. Relaxation and fluctuations of membrane currents that flow through drug-operated channels. *Proc. R. Soc. Lond. B Biol. Sci.* 199:231–262.

Colquhoun, D., and A.G. Hawkes. 1981. On the stochastic properties of single ion channels. *Proc. R. Soc. Lond. B Biol. Sci.* 211:205–235.

Connors, B.W., M.J. Gutnick, and D.A. Prince. 1982. Electrophysiological properties of neocortical neurons in vitro. *J. Neurophysiol.* 48:1302–1320.

Crill, W.E. 1996. Persistant sodium current in mammalian central neurons. *Annu. Rev. Physiol.* 58:349–362.

Cummins, T.R., J.R. Howe, and S.G. Waxman. 1998. Slow closed-state inactivation: a novel mechanism underlying ramp currents in cells expressing the hNE/PN1 sodium channel. *J. Neurosci.* 18: 9607–9619.

Cummins, T.R., Y. Xia, and G.G. Haddad. 1994. Functional properties of rat and human neocortical voltage-sensitive sodium currents. *J. Neurophysiol.* 71:1052–1064.

D'Angelo, E., G. De Filippi, P. Rossi, and V. Taglietti. 1998. Ionic mechanism of electroresponsiveness in cerebellar granule cells implicates the action of a persistent sodium current. *J. Neurophysiol.* 80:493–503.

Deisz, R.A., G. Fortin, and W. Zieglgänsberger. 1991. Voltage dependence of excitatory postsynaptic potentials of rat neocortical neurons. *J. Neurophysiol.* 65:371–382.

Dickson, C.T., and A. Alonso. 1997. Muscarinic induction of synchronous population activity in the entorhinal cortex. *J. Neurosci.* 17:6729–6744.

Doyère, V., and S. Laroche. 1992. Linear relationship between the maintenance of hippocampal long-term potentiation and retention of an associative memory. *Hippocampus*. 2:39–48.

Fan, S., M. Stewart, and R.K. Wong. 1994. Differences in voltage-dependent sodium currents exhibited by superficial and deep layer neurons of pig entorhinal cortex. *J. Neurophysiol.* 71:1986–1991.

Fleidervish, I.A., and M.J. Gutnick. 1996. Kinetics of slow inactivation of persistent sodium current in layer V neurons of mouse neocortical slices. *J. Neurophysiol.* 76:2125–2130.

Franceschetti, S., E. Guatteo, F. Panzica, G. Sancini, E. Wanke, and G. Avanzini. 1995. Ionic mechanisms underlying burst firing in pyramidal neurons: intracellular study in rat sensorimotor cortex. *Brain Res.* 696:127–139.

French, C.R., and P.W. Gage. 1985. A threshold sodium current in pyramidal cells in rat hippocampus. *Neurosci. Lett.* 56:289–293.

French, C.R., P. Sah, K.J. Buckett, and P.W. Gage. 1990. A voltage-dependent persistent sodium current in mammalian hippocampal neurons. *J. Gen. Physiol.* 95:1139–1157.

Greenstein, Y.J., C. Pavlides, and J. Winson. 1988. Long-term potentiation in the dentate gyrus is preferentially induced at theta rhythm periodicity. *Brain Res.* 438:331–334.

Hamill, O.P., A. Marty, E. Neher, B. Sakmann, and F.J. Sigworth. 1981. Improved patch-clamp techniques for high-resolution current recording from cells and cell-free membrane patches. *Pflügers Arch.* 391:85–100.

Hodgkin, A.L., and A.F. Huxley. 1952. A quantitative description of membrane current and its application to conduction and excitation in nerve. *J. Physiol.* 117:500–544.

Holmes, J.E., and W.R. Adey. 1960. Electrical activity of the entorhinal cortex during conditioned behaviour. *Am. J. Physiol.* 199:741–744.

Hölscher, C., R. Anwyl, and M.J. Rowan. 1997. Stimulation on the positive phase of hippocampal theta rhythm induces long-term potentiation that can be depotentiated by stimulation on the negative phase in area CA1 in vivo. *J. Neurosci.* 17:6470–6477.

Hotson, J.R., D.A. Prince, and P.A. Schwartzkroin. 1979. Anomalous inward rectification in hippocampal neurons. *J. Neurophysiol.* 42:889–895.

Huerta, P.T., and J.E. Lisman. 1996. Low-frequency stimulation at the troughs of 2-oscillation induces long-term depression of previously potentiated CA1 synapses. *J. Neurophysiol.* 75:877–884.

Huguenard, J.R., O.P. Hamill, and D.A. Prince. 1988. Developmental changes in Na^+ conductances in rat neocortical neurons: appearance of a slowly inactivating component. *J. Neurophysiol.* 59: 778–795.

Jahnsen, H. 1986. Extracellular activation and membrane conductances of neurones in the guinea-pig deep cerebellar nuclei in vitro. *J. Physiol.* 372:149–168.

Jahnsen, H., and R. Llinás. 1984. Ionic basis for the electro-responsiveness and oscillatory properties of guinea-pig thalamic neurones in vitro. *J. Physiol.* 349:227–247.

Ju, Y.K., D.A. Saint, and P.W. Gage. 1994. Inactivation-resistant channels underlying the persistent sodium current in rat ventricular myocytes. *Proc. R. Soc. Lond. B Biol. Sci.* 256:163–168.

Kay, A.R., R. Miles, and R.K. Wong. 1986. Intracellular fluoride alters the kinetic properties of calcium currents facilitating the investigation of synaptic events in hippocampal neurons. *J. Neurosci.* 6:2915–2920.

Kay, A.R., M. Sugimori, and R. Llinás. 1998. Kinetic and stochastic properties of a persistent sodium current in mature guinea pig cerebellar Purkinje cells. *J. Neurophysiol.* 80:1167–1179.

Klink, R., and A. Alonso. 1993. Ionic mechanisms for the subthreshold oscillations and differential electroresponsiveness of medial entorhinal cortex layer II neurons. *J. Neurophysiol.* 70:144–157.

Klink, R., and A. Alonso. 1997. Morphological characteristics of layer II projection neurons in the rat medial entorhinal cortex. *Hippocampus*. 7:571–583.

Larson, J., and G. Lynch. 1986. Induction of synaptic potentiation in hippocampus by patterned stimulation involves two events. *Science.* 232:985–988.

Larson, J., D. Wong, and G. Lynch. 1986. Patterned stimulation at the theta frequency is optimal for the induction of hippocampal long-term potentiation. *Brain Res.* 368:347–350.

Lipowsky, R., T. Gillessen, and C. Alzheimer. 1996. Dendritic Na^+ channels amplify EPSPs in hippocampal CA1 pyramidal cells. *J. Neurophysiol.* 76:2181–2191.

Llinás, R.R., and A. Alonso. 1992. Electrophysiology of the mammillary complex in vitro. I. Tuberomammillary and lateral mammillary neurons. *J. Neurophysiol.* 68:1307–1320.

Llinás, R., and M. Sugimori. 1980. Electrophysiological properties of in vitro Purkinje cell somata in mammalian cerebellar slices. *J. Physiol.* 305:171–195.

Ma, J.Y., W.A. Catterall, and T. Scheuer. 1997. Persistent sodium currents through brain sodium channels induced by G protein betagamma subunits. *Neuron*. 19:443–452.

Magistretti, J., and M. de Curtis. 1998. Low-voltage activated T-type calcium currents are differently expressed in superficial and deep layers of guinea pig piriform cortex. *J. Neurophysiol.* 79:808–816.

Magistretti, J., D.S. Ragsdale, and A. Alonso. 1999. High conductance sustained single channel activity responsible for the low threshold persistent Na^+ current in entorhinal cortex neurons. *J. Neurosci.* 19:7334–7341.

Masukawa, L.M., A.J. Hansen, and G. Shepherd. 1991. Distribution of single-channel conductances in cultured rat hippocampal neurons. *Cell. Mol. Neurobiol.* 11:231–243.

Mitchell, S.J., and J.B. Ranck, Jr. 1980. Generation of theta rhythm in medial entorhinal cortex of freely moving rats. *Brain Res.* 189: 49–66.

Nisenbaum, E.S., C.J. Wilson, R.C. Foehring, and D.J. Surmeier. 1996. Isolation and characterization of a persistent potassium current in neostriatal neurons. *J. Neurophysiol.* 76:1180–1194.

Pape, H.C., and R.B. Driesang. 1998. Ionic mechanisms of intrinsic oscillations in neurons of the basolateral amygdaloid complex. *J. Neurophysiol.* 79:217–226.

Parri, H.R., and V. Crunelli. 1998. Sodium current in rat and cat thalamocortical neurons: role of a non-inactivating component in tonic and burst firing. *J. Neurosci.* 18:854–867.

Pennartz, C.M., M.A. Bierlaagh, and A.M. Geurtsen. 1997. Cellular mechanisms underlying spontaneous firing in rat suprachiasmatic nucleus: involvement of a slowly inactivating component of sodium current. *J. Neurophysiol.* 78:4811–4825.

Ragsdale, D.S., and M. Avoli. 1998. Sodium channels as molecular targets for antiepileptic drugs. *Brain Res. Brain Res. Rev.* 26:16–28.

Ramón y Cajal, S. 1902. Sobre un ganglio especial de la corteza esfeno-occipital. *Trab. del Lab. de invest. Biol. Univ. Madrid.* 1:189–201.

Sah, P., A.J. Gibb, and P.W. Gage. 1988. The sodium current underlying action potentials in guinea pig hippocampal CA1 neurons. *J. Gen. Physiol.* 91:373–398.

Schwindt, P.C., and W.E. Crill. 1995. Amplification of synaptic current by persistent sodium conductance in apical dendrite of neocortical neurons. *J. Neurophysiol.* 74:2220–2224.

Segal, M.M. 1994. Endogenous bursts underlie seizurelike activity in solitary excitatory hippocampal neurons in microcultures. *J. Neurophysiol.* 72:1874–1884.

Stafstrom, C.E., P.C. Schwindt, M.C. Chubb, and W.E. Crill. 1985. Properties of persistent sodium conductance and calcium conductance of layer V neurons from cat sensorimotor cortex in

vitro. *J. Neurophysiol.* 53:153–170.
Stafstrom, C.E., P.C. Schwindt, and W.E. Crill. 1982. Negative slope conductance due to a persistent subthreshold sodium current in cat neocortical neurons in vitro. *Brain Res.* 236:221–226.
Steward, O., and S.A. Scoville. 1976. Cells of origin of entorhinal cortical afferents to the hippocampus and fascia dentata of the rat. *J. Comp. Neurol.* 169:347–370.
Stuart, G., and B. Sakmann. 1995. Amplification of EPSPs by axosomatic sodium channels in neocortical pyramidal neurons. *Neuron*. 15:1065–1076.
Taylor, C.P. 1993. Na^+ currents that fail to inactivate. *Trends Neurosci*. 16:455–460.
Taylor, C.P., and B.S. Meldrum. 1995. Na^+ channels as targets for neuroprotective drugs. *Trends Pharmacol. Sci*. 16:309–316.
Uteshev, V., D.R. Stevens, and H.L. Haas. 1995. A persistent sodium current in acutely isolated histaminergic neurons from rat hypothalamus. *Neuroscience.* 66:143–149.
van der Linden, S., and F.H. Lopes da Silva. 1998. Comparison of the electrophysiology and morphology of layers III and II neurons of the rat medial entorhinal cortex in vitro. *Eur. J. Neurosci.* 104:1479–1489.
White, J.A., A. Alonso, and A.R. Kay. 1993. A heart-like Na^+ current in the medial entorhinal cortex. *Neuron* 11:1037–1047.